Field-Directed Nanowire Chaining Enabling Transparent Electrodes

by

Manyan Xu
B.Eng., Zhejiang University, China, 2016

A Thesis Submitted in Partial Fulfillment
of the Requirements for the Degree of

MASTER OF APPLIED SCIENCE

in the Department of Mechanical Engineering

University of Victoria

Supervisory Committee

Field-Directed Nanowire Chaining Enabling Transparent Electrodes

by

Manyan Xu
B.Eng., Zhejiang University, China, 2016

Supervisory Committee

Dr. Rustom Bhiladvala, Department of Mechanical Engineering

Supervisor

Dr. Mohsen Akbari, Department of Mechanical Engineering

Departmental Member

Abstract

Supervisory Committee

Dr. Rustom Bhiladvala, Department of Mechanical Engineering

Supervisor

Dr. Mohsen Akbari, Department of Mechanical Engineering

Departmental Member

Transparent electrodes (TEs) require materials that have both transparency and electrical conductivity, a combination not usually found in nature. They are in increasing demand for use in solar cells, touch screens, displays, transparent heating films and several other devices. Most TEs used today are made of indium tin oxide (ITO). However, it has several disadvantages, such as high fabrication cost, rigidity and brittleness. Many ITO alternatives are being pursued, among which metallic nanowire (NW) networks on transparent substrates such as glass or polymer, have received much attention. This thesis demonstrates ordered silver NW networks on polyimide, fabricated by the field-directed chaining technique. We achieved a sheet resistance of 27 Ω/sq and 95.4% transparency at 550nm, with a Figure of Merit (FOM) $0.023\Omega^{-1}$, which is higher than the FOM of commercial ITO, $0.005\Omega^{-1}$. We have demonstrated that ordered NW networks, directed by alternative current (AC) electric fields, are easy to fabricate over a large area and at low cost, on rigid and flexible substrates.

The AC electric field changes with different experiment setup. In this work, the effect of polymer thickness, electric field frequency, and gap size between electrodes are explored by COMSOL simulation and validated experimentally. By choosing the appropriate frequency and gap size, ordered NW networks are successfully created on a 23μm polyethylene terephthalate (PET) sheet. Fluid motion is one of the disruptors during NW chaining. We demonstrate control of this disruptor by the use of sandwiched channels for the NW suspension.

Post-fabrication treatments are important and necessary for improving the connectivity and conductivity of Ag NW networks. In this work, we explore Joule heating and show its potential to

improve the conductivity over other post-treatment approaches. However, Joule heating can also cause failures of NW networks.

Ordered NW networks present better optical-electrical properties than random NW networks. Post-fabrication treatment can improve the properties, but there is a limit. In this work, a mathematical model is built for optical-electrical properties of perfectly ordered NW networks, which sets the upper bound of performance for transparent electrodes made of NW networks. A linear relationship is found between the transmittance and inverse sheet resistance. The model is then modified with factors to account for departure from the ideal.

Table of Contents

List of Tables

List of Figures

List of Acronyms

NW	Nanowire
Ag NW	Silver nanowire
TEs	Transparent electrodes
%T	Transparency
Rs	Sheet resistance
ITO	Indium tin oxide
TCOs	Transparent conducting oxides
NCTs	Carbon Nanotubes
PEDOT: PSS	Poly(3,4-ethylenedioxythiophene) poly(styrenesulfonate)
EG	Ethylene glycol
PVP	Poly(vinyl pyrrolidone)
FOM	Figure of Merit
IPA	Isopropyl Alcohol

Acknowledgments

I would like to express my gratitude to the people that helped me make the completion of this work possible.

The most important acknowledgement of my gratitude that I want to express is to my supervisor, Dr. Rustom Bhiladvala, for giving me this opportunity, and his guidance through the journey of my graduate studies. He has shared his deep knowledge with me, inspired me when I was stuck with my research, and also gave me the freedom to pursue new ideas. I also want to extend my thanks to my committee members Dr. Mohsen Akbari and Dr. Tao Lu.

Dr. Sahar Sam has taught me a lot of knowledge and experimental skills. I want to thank her for working with me and sharing her knowledge and skills, and always giving me useful advice when I needed help.

Thanks to CAMTEC for letting me use their facilities. Thanks to Dr. Elaine Humphery for teaching me how to use the SEM as well as helping me use It. Thanks to Jon Rudge for helping me use the clean room and the nanofabrication tools. Thanks to Dr. Alex Brolo for the use of his lab.

I also want to thank all the students in my research team Jehad, Vinayak, Dana, Leah, Zhuoqun, Padmini, and Amin, for all their support, help, and friendship.

Last but not least, I will always be thankful to my family for the unconditional love and support. And I want to thank my boyfriend Jack for always being there when I needed help and in my low moments.

Dedication

To my beloved parents: Maosu and Jingrong

Chapter 1 Introduction

1.1 Transparent electrodes

Transparent electrodes are materials that have both transparency and electrical conductivity. They are growing in demand because they are widely used in modern devices, such as solar cells [1], touch screens [2], liquid crystal displays (LCDs) [3], multi-functional windows [4], and transparent heating films [5]. In solar cells, sunlight needs to pass through the top electrode to reach the semiconductor material to generate charge carriers; at the same time, the charge carries generated in the semiconductor material need to be transported through the electrodes to reach the load in the circuit. Therefore, solar cells require at least one of the electrodes to be transparent to perform normally. Figure 1.1 shows the architecture of an organic solar cell, in which ITO deposited on glass serves as a transparent anode. Transparent electrodes in solar cells require a wider range of transparency than other applications to make better use of the energy in the solar spectrum.

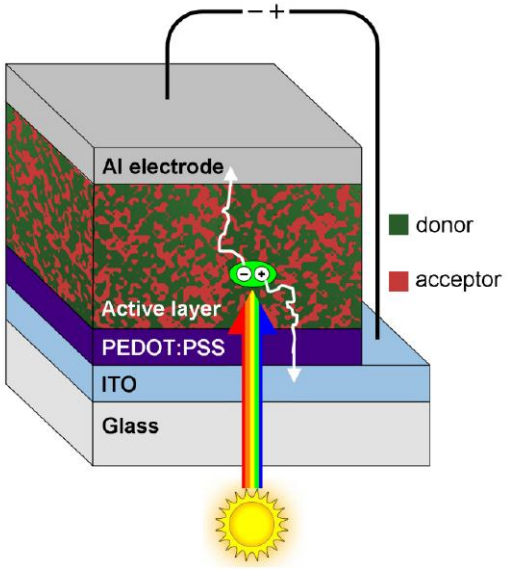

Figure 1.1 Architecture of an organic solar cell, in which ITO serves as a transparent electrode [1]**.**

In addition, transparent electrodes are used in touchscreens for high-resolution televisions, smartphones, tablets, computers and laptops. There are several different touchscreen technologies, among which resistive touchscreen and capacitive touchscreens are most

commonly used, and both require transparent electrodes [2]. A resistive touchscreen has two transparent conductive layers facing each other with a small gap in between to sense the position of pressure on the screen. A capacitive touchscreen also consists of two layers of transparent electrodes, positioned in X and Y directions, to measure the change in capacitance and to determine the touched location. Figure 1.2 demonstrates the layers in a capacitive touchscreen, in which ITO are used as transparent electrodes.

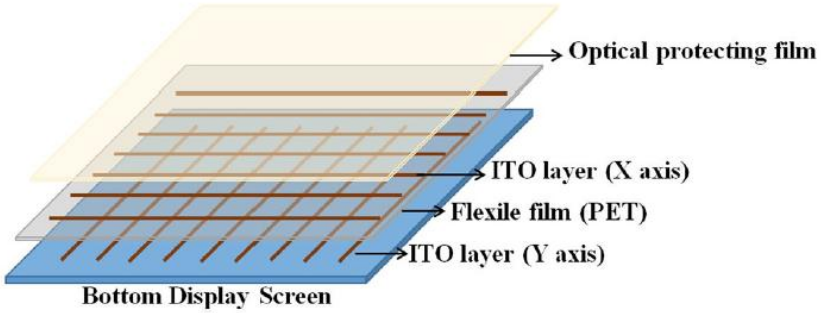

Figure 1.2 Schematic of structures in a capacitive touchscreen, in which ITO are positioned in X and Y axis as transparent electrodes [6]**.**

In LCDs, pixels consist of a layer of molecules aligned between two transparent electrodes and two polarizing filters [3]. Transparent heating films use transparent electrodes to generate heat, and they are usually used to defrost cameras, car windows, or goggles in cold weather.

1.1.1 Transparent conductive materials probably do not naturally exist

Transparency and conductivity are two very common properties of materials. There is a large number of conductive materials and many kinds of transparent materials in our daily life, but it is very likely the transparent materials do not naturally exist.

For a material to be transparent, it has to have a band gap which does not lead to significant absorption in the wavelength range of the visible light spectrum. The visible part of solar spectrum lies within the energy range of 1.8-3.4 eV [7]. Therefore, a transparent material should have a band gap greater than 3.4 eV. Alternatively, for a material to be conductive, it must have no gap at the Fermi Level, like metals, or doped semiconductors, such as n-

type or p-type silicon. The conductivity of doped semiconductors can be increased either by doping the material heavily, or by increasing the mobility of the material. However, these methods of increasing the conductivity usually do not go hand in hand with the transparency property. When the band gap is lower, the material begins to absorb photons. Alternatively, when the doping is increased, the material increases the free carrier absorption; both methods lower the transparency.

1.1.2 ITO

The most widely used transparent conductive electrodes currently are made of indium tin oxide (ITO). ITO is a heavily doped n-type semiconductor. Its bandgap is about 3.5 eV to 4.3 eV. It is almost totally transparent in the visible wavelength because of this large bandgap. In the ultraviolet spectral range, it is opaque due to the band-to-band absorption. Band-to-band absorption happens when the high energy photon excites the electron from the valence band to the conduction band. In the infrared and near infrared range, ITO is also opaque because of free carrier absorption. Free carrier absorption happens when the low energy photon excites the electron from near the bottom of the conduction band to far from the conduction edge [8]. It has excellent opto-electrical properties with about 90% of transparency at a sheet resistance of 10-25 Ω/sq [9].

However, ITO has several disadvantages. First, Indium is a scarce resource and its ever-rising consumption and demand result in its increasingly volatile price. Figure 1.3 shows the Indium price over the past few decades. The price has large volatility, which negatively impacts manufacturers. Second, ITO is rigid and brittle, thus it is not suitable for flexible electronics. Third, the deposition of ITO needs a vacuum environment and often a high temperature. Therefore, alternatives to ITO as transparent conductive electrodes are urgently needed.

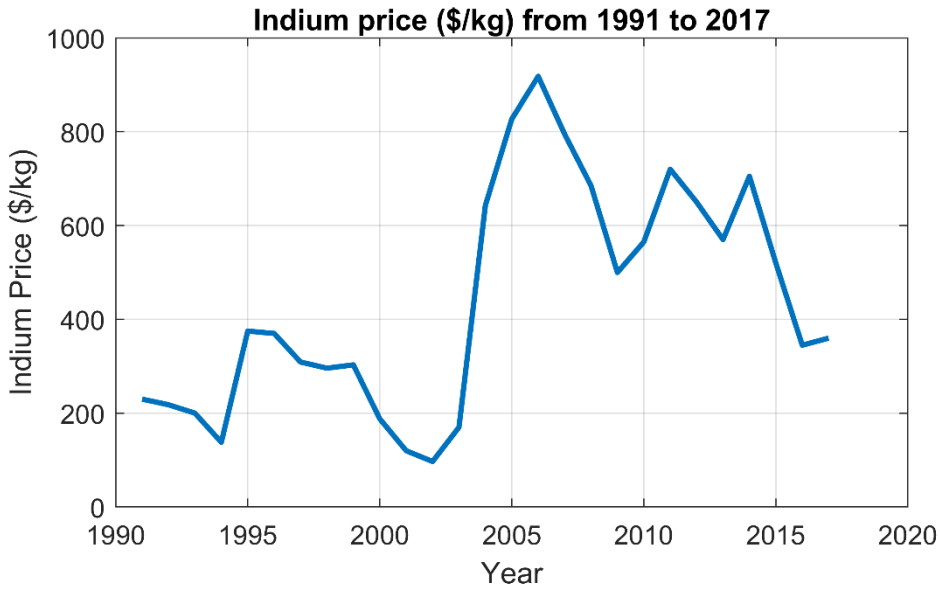

Figure 1.3 The volatility of Indium price from 1991 to 2017 [10]

Due to the demand of TEs and drawbacks of ITO, many alternative materials are being pursued, which will be introduced in Chapter 2. The ITO alternative we researched is a network of metallic NWs on a transparent substrate. The metallic NWs can conduct currents, which makes the combined material conductive. At the same time, light can pass through the holes among NWs, which makes the material transparent. The order of the NW configuration is enabled using the NW chaining technique, directed by an AC electric field. We call the resultant TEs ordered NW networks. Field directed NW chaining for TE applications was established for the first time by our previous PhD student, Mahshid Sam [11]. NW chaining on rigid and polymeric substrates were demonstrated. After that, a parametric study of ordered NW networks on rigid substrates was conducted by our previous Master student, Jehad Alsaif [12]. The detailed fabricating method will be presented in Chapter 2. Figure 1.4 shows an example of ordered NW networks [13]. Their optical-electrical properties are comparable to ITO. In addition, they can be processed inexpensively and has the potential to be produce over large area at low cost.

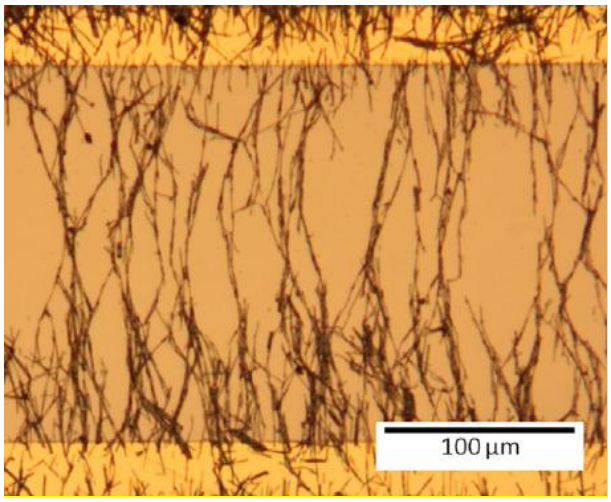

Figure 1.4 An optical micrograph of ordered NW networks created on glass substrate by NW chaining technique [13]**. NWs used are Rh NWs, and two yellow rectangles at the top and bottom are gold electrodes, through which the electric field was applied in the fabrication process**

1.2 Contributions of this thesis

This thesis focuses on studying ordered NW networks for application to transparent electrodes, especially on flexible substrates. The contributions of this thesis include:

1. Improved performance of ordered NW networks. This was achieved by exploring post-fabrication treatment to improve conductivity of NW-junctions, as well as designing tools to supress disruption due to fluid movement in the NW chaining process.
2. Evaluation of the effects of field frequency, polymer thickness and assembly electrode gap size on the electric field used to direct NW chaining. This was achieved by parametric studies carried out through experiments and numerical simulations.
3. Creation of a model describing the electrical and optical properties of ordered NW networks for both ideal and practical scenarios. This was done by modelling based on reasonable assumptions.

1.3 Thesis structure

This thesis presents a method of fabricating transparent electrodes using NW chaining technique, and related material exploration and modelling. There is no separate chapter for literature review, methods, or experiment in this thesis. This information is presented in each section where needed, or in the Appendices if it is too long.

Chapter 2 explains the choice of pursuing ordered NW networks from the many ITO alternatives. The method of using NW chaining to fabricate transparent electrodes is then introduced. The characteristic of the fabricated transparent electrodes is presented and compared with other TEs reported. A mathematical model is presented for optical-electrical properties of perfectly ordered NW networks, which set the upper bound of performance for transparent electrodes made of NW networks. The factors that account for departure from the ideal scenario are discussed and a modified model for fabricated ordered NW networks is presented.

Chapter 3 explores a post-treatment method, Joule heating, to improve the conductance of ordered NW networks. The difference of Joule heating between a chained section and branched section is discussed. The effect, limitation and risk of using Joule heating as post-treatment are shown by experiments, and suggestions of how Joule heating should be used for improvement and lowering failure risk are given.

Chapter 4 presents the change of polymer on which NW ordered networks are deposited. The effect of polymer thickness and electrical properties on electric field is demonstrated through COMSOL simulations. NW ordered networks on a 23 μm thick PET sheet are shown by experiments.

Chapter 5 demonstrates an approach of sandwiched channels to limit the influence of liquid motion during the NW chaining process. Results of NW ordered networks using this method are presented. Limitations and further improvement suggestions are given.

Chapter 6 summarizes the work done in this Master research and gives suggestions for future work in this field.

Chapter 2 Field directed nanowire chaining for transparent electrodes: fabrication & characterization

This chapter introduces different approaches of available TEs and presents the basis and process of the NW chaining technique. The performance of the fabricated ordered NW networks is compared to the other TEs reported. Models for the ordered NW networks are built towards the end of the chapter.

2.1 Introduction for ITO alternatives

Due to the high demands of TEs and the drawbacks of ITO, there is a strong research effort directed to the search for alternative materials. The study of ITO alternatives can be categorized into four groups: transparent conducting oxides (TCOs), nanostructured carbon, conductive polymers, and metallic nanostructures. The ordered NW networks studied in this thesis belongs to the group of metallic nanostructures.

2.1.1 Other transparent conducting oxides (TCOs)

TCOs are the earliest group for TEs, and were dominant in the field for decades after World War II [14]. They are a class of thin film metal oxides doped with other materials which adjusts their transparency and conductivity. The metal oxides explored in researches include In_2O_3, SnO_2, ZnO, CdO, CdO, TiO_2 and Cu_2O [15]. Besides doped In_2O_3, doped SnO_2 and ZnO gain the most attention because of their high bandgap energy allows high transparency in the visible and near-ultraviolet region [15]. Popular TCOs in research and industrial applications as TEs include tin oxide doped with fluorine (SnO_2:F), and tin oxide doped with antimony (ATO), zinc oxide doped with fluorine (ZnO:F), and zinc oxide doped with aluminum (AZO) [16]. The optical and electrical properties of TCOs depends on the metal oxides, dopant content, dopant concentrations, post-treatment and film thickness. For example, the sheet resistance of ATO thin films range between 100-1400 Ω/sq, and their transparency ranges from 80% to 95% [17].

There are two general drawbacks of TCOs as TE. First, TCOs are brittle and often crack or break with small strains, so are not appropriate for flexible photoelectronic devices.

Second, the fabrication of TCOs usually include deposition of chemical vapor deposition (CVD) or sputtering, which is expensive and requires a high vacuum environment [14].

2.1.2 Nanostructured carbon

Carbon nanotubes (CNTs) and graphene are two carbon allotropes that show great promise in the field of transparent conductive electrodes [18]. They are both made of a meshwork of sp^2-hybridized carbon atoms but with different structures. Single walled CNTs have the cylindrical structures that are formed by rolling up graphene, while graphene is a 2-dimensional flat sheet [18]. Compared to ITO, CNTs and graphene are stronger and more flexible, chemically stable, and have the potential for low cost fabrication since carbon is one of the most abundant elements on earth. To fabricate transparent conductive graphene films, CNTs can be applied to surfaces from purified CNT inks, which is one of the main advantages of CNTs compared to ITO [19]. Graphene sheets can be transferred onto different kinds of transparent substrates by physical contact printing [20] and chemical etching processes [21].

The electrical conductivity of CNTs and graphene is anisotropic. For single-walled CNTs, they are highly conductive only along their axes. For graphene, it is highly conductive only within the graphene sheet. The contact resistance between CNTs or graphene sheets is very high [18]. Therefore, if the conducting pathway has to pass through several CNTs or graphene sheets, the electrical conductance of the network will drop greatly. Ideally, a single large size graphene sheet has the transmittance of about 97.7% and the sheet resistance of about 60 Ω/sq. However, typically a graphene network produced from solution processes has a sheet resistance of about 2000 Ω/sq when transmittance is about 85% [22]. Theoretically, the highest conductance of a SWNT network is about 10 Ω/sq when the transmittance is about 92% [23]. The highest conductance of SWNTs achieved is 60 Ω/sq, when the transmittance is 90.9% [24].

2.1.3 Transparent conductive polymers

Compared to most of the other transparent conductive materials, transparent conducting polymers have many strengths, such as excellent mechanical flexibility, low cost, light weight, and strong compatibility with plastic substrates. Currently, the most popular

transparent conducting polymer is poly(3,4-ethylenedioxythiophene): poly(styrene sulfonate) (PEDOT:PSS), which has its chemical structure is shown in Figure 2.1 [25].

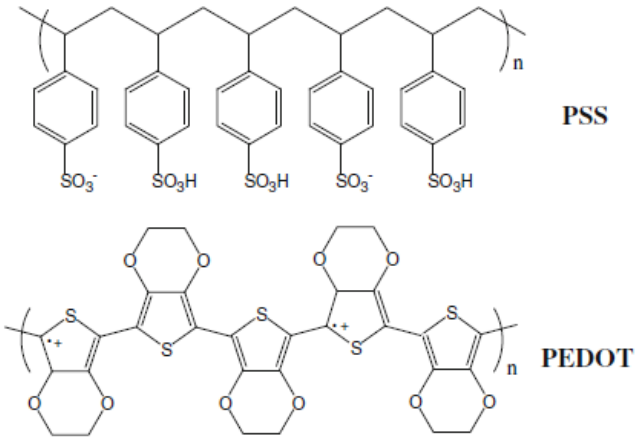

Figure 2.1 Chemical structure of PEDOT:PSS [25]

One of the major drawbacks of transparent conductive polymers is their low electrical conductivity, which makes them not ideal ITO alternatives in many applications. PEDOT:PSS directly prepared from solution have rather low electrical conductivity of less than 10 S/cm, thus their conductivity needs to be improved for them to be used as transparent conductive electrodes [25]. Their conductivity can be enhanced by adding other materials in post-treatment. For example, it is reported that after three treatments of H_2SO_4, the conductivity of PEDOT:PSS reaches 3065 S/cm [26]. However, acid treatment is corrosive and hard to control. Increasing film thickness also improves conductivity, but the transparency will decrease. According to Zhang et al. [27], when the film thickness increases from 78nm to 300nm, the sheet resistance decreases from 250Ω/sq to 75Ω/sq, but the transparency decreases from about 95% to 65%. Another problem of conductive polymers is their instability in air. The electrical property of PEDOT:PSS degrades rapidly in air because of their absorption of moisture and oxygen [25].

Although it is difficult to use conductive polymers themselves as ITO alternatives, researches have shown that they can be combined with nanostructured metals [28, 29] or graphene [30] to improve the overall conductivity.

2.1.4 Metallic nanostructures

Metals are amongst the most conductive materials on earth, but they are generally opaque in the visible range of light. Because of the opacity, fabricating transparent metallic materials was very difficult until the emergence and development of nanotechnology. There are three approaches to achieve transparent metallic electrodes: ultrathin metal films, metal nanoscale grids, and NW networks [19]. The ordered NW networks studied in this thesis belong to the last category.

Ultrathin metal films

Ultrathin metal films require a thickness of about 10 nm or less to lower the light scattered and become transparent in the visible spectral range [31]. The metals for ultrathin metal films can be single-component metals such as nickel or chromium, multi-component metals or metal alloys. As the materials become thinner, their transparency increases but conductance deceases. Figure 2.2 shows how the film thickness affect the optical and electrical properties of ultrathin Cr and Ni films. The transparencies of ultrathin metal films are relatively low compared to ITO [31]. Additionally, ultrathin films undergo an expensive process which involves fabrication via sputtering metals in ultra high vacuum chambers [19].

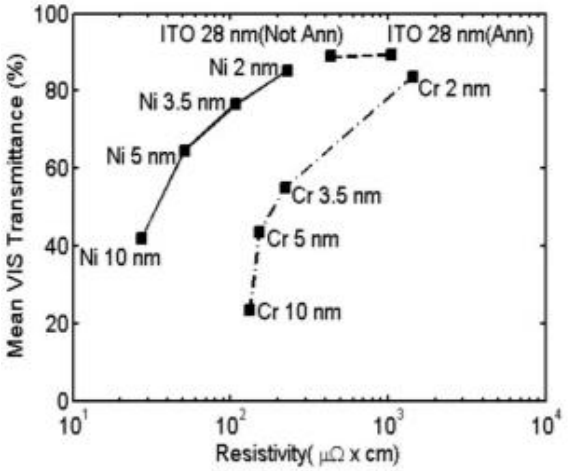

Figure 2.2 Mean transmittance in the visible wavelengths and resistivity of ultrathin Cr and Ni films compared with annealed and unannealed ITO [31]

Metal nanoscale grids

Metal nanoscale grids have holes that are totally transparent. The overall transmittance is determined by the percentage of area that is covered by the metal grid. The line thickness affects the conductance [32]. They are usually fabricated by electron beam lithography or nanoimprint lithography. Figure 2.3 shows Platinum nanoscale grids patterned by nanoimprint lithography, and their sheet resistance is about 100 Ω/sq with 89% transparency [33].

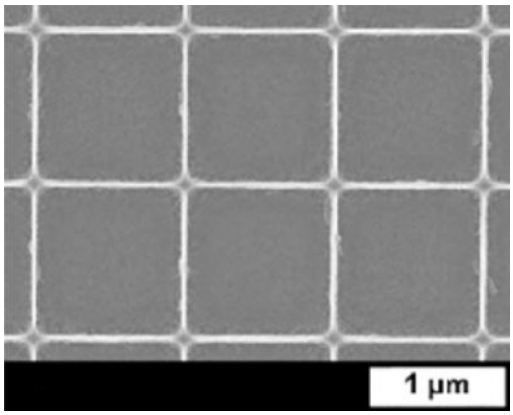

Figure 2.3 Platinum nanoscale grids on glass with line width of 40 nm, fabricated by nanoimprint lithography [33]

Metal nanoscale grids can have high optical and electrical properties that are comparable to ITO. Metal nanoscale grids fabricated by electron beam lithography show a sheet resistance of 6.5Ω/sq with 91% transparency [34]. However, their main problems are high cost to fabricate and difficult to produce at large scale.

Metallic NW networks

Metallic NW networks are generally fabricated by deposited NWs on transparent substrates. NWs can be considered as one-dimensional nanostructures, which have diameters of around 100nm or less, and lengths of 1µm or longer. For NWs with diameters of tens of nm or larger, electrical conductivity along the length of NWs behaves similar to that of the bulk metal [35]. Thus, well-connected NW networks can transport charges effectively. The uncovered area in NW networks allows light to pass through freely while some light scattered by NWs travels forward through the networks [36]. Figure 2.4 shows

an examples of random Ag NW networks [37]. Generally, the optical and electrical properties of NW networks are affected by NW density; the denser NWs leads to higher conductivity and lower transparency, and vice versa. NW networks can achieve sheet resistance of 10s Ω/sq or lower with transparency of 90% or higher [38][39], which is comparable to ITO.

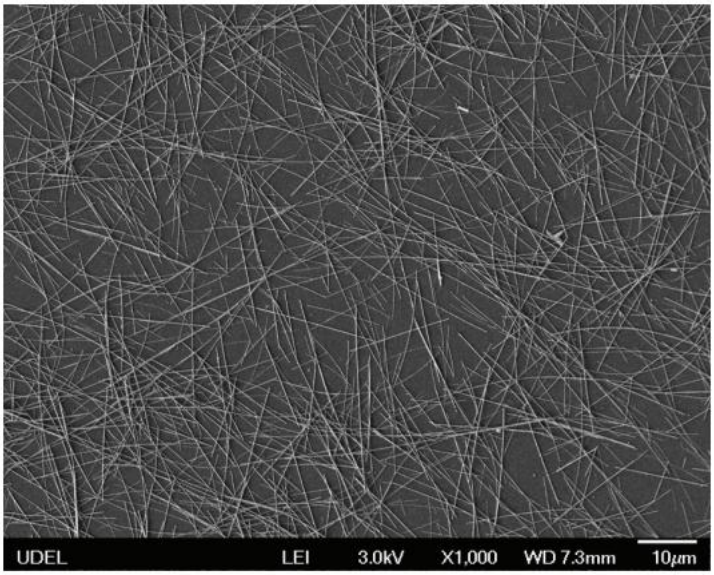

Figure 2.4 Scanning Electron Microscope (SEM) image of random NW networks fabricated on glass by dip coating [37]**.**

A variety of NW materials and fabricating methods have been explored in literature. Silver attracts the most widespread interest as the material for metallic NW networks because it is the most electrically conductive metal. NWs networks of other metals, such as Cu [29], Au [40], Rh [12] have also been researched. NW networks can be fabricated from solution by many methods, including drop casting, spin coating, spray coating [39][41], dip costing [37], and Meyer rod coating [38]. Fabricating from solution means low cost for mass production. Among the ITO alternatives reviewed above, metallic NW network is the only one that can both be solution-processed and perform competitively to ITO. Ordered NW networks researched in this thesis belongs to the category of metallic NW networks. NW chaining technique controls the connection of NWs, which is absent in random NW networks.

2.1.5 Advantages of ordered NW networks compared to random NW networks

There is no control over NW connection in random NW networks, and the orientation of NWs are unpredictable. Ordered NW networks have NWs connected in a preferable direction. The advantages of this can be understood by a metaphor of electrons passing in the NW network to cars travelling on roads.

The passing of current through NW paths from one end to the other can be viewed as cars driving on roads from the start position to their destination. There are fewer lanes at the intersection from one road to the other, to mimic the small contact area at the NW junctions. Figure 2.5 demonstrates a random network and an ordered network connecting the start and end pads. An ordered network is like roads built in the desired direction, which will allow the car to arrive at the destination with the least effort and time. However, a random network is like roads built in many different directions requiring a longer travel distance and more road changes needed to reach the destination. This will take more effort and time, meaning a higher resistance in the NW networks. In addition, with the same number of NWs, more paths connect two ends if the direction is controlled, which contributes to lower resistance. It will take more NWs for a random network to reach the same number of connected paths, which will lower the transparency.

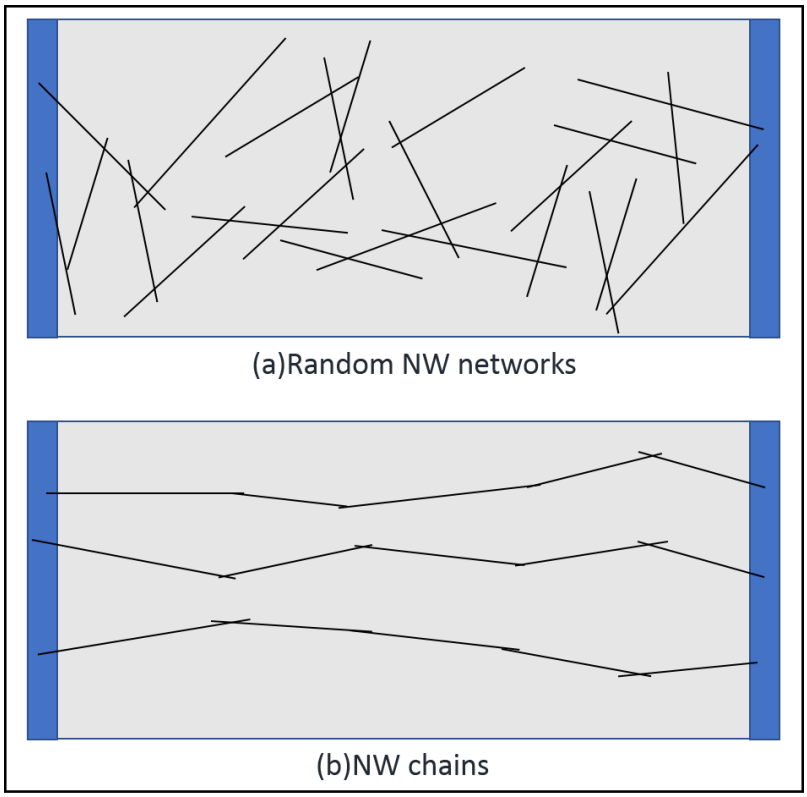

Figure 2.5 Illustrations of NW path from one side to the other in (a) random networks and (b) ordered networks made of NW chains. In the random networks, a longer path and more junctions are required to reach the other side than in the ordered networks.

In summary, compared with a random NW network, an ordered NW network requires fewer NWs to reach the same resistance, and has higher transparency, which means overall better quality for transparent electrodes. NWs are the most expensive parts in NW networks. We choose to fabricate ordered NW networks for their higher quality and lower cost.

2.2 Theory for the NW chaining technique

NWs are directed by three effects of an electric field: force due to dielectrophoresis (DEP) drags NWs towards the electrodes; torques caused by dipole moments rotate the NWs to align them with the electric field direction; dipole-dipole interaction connects the NWs into chains.

2.2.1 Directed effects of the electric field

DEP is the translational motion experienced by dipolar particles in the direction of the field gradient, caused by a nonuniform electric field [42]. Assuming NWs have cylindrical shapes, the expression of the DEP force for a NW in a nonuniform electric field is [42]:

$$F_{DEF} = \frac{\pi r^2 l}{6} \varepsilon_m Re(F_{CM}) \nabla(E^2), \quad (1)$$

in which r and l is the radius and length of the NW; ε_m is the medium permittivity, E is the electric field; and $Re(F_{CM})$ is the real part of the Clausius-Mossotti factor F_{CM}, which depends on the frequency and the permittivity of the medium and NWs, and is defined as [42]:

$$F_{CM} = \frac{\varepsilon^*_{NW} - \varepsilon^*_m}{\varepsilon^*_m}, \quad (2)$$

ε^*_m and ε^*_{NW} are the complex permittivities of the medium and the NW, respectively. Complex permittivity is defined as $\varepsilon^* = \varepsilon - j(\frac{\sigma}{\omega})$, in which σ is the electrical conductivity and ω is the angular frequency of the electric field. There are negative DEP and positive DEP, depending on the sign of $Re(F_{CM})$. Negative DEP causes particles to move towards regions with lower field strengths, while positive DEP causes particles to move towards regions with higher field strengths. For metallic NWs in alcohol, because the conductivity and permittivity of the metallic NWs are much larger than those of alcohol, DEP below 10^{10} Hz is generally positive [13, 45].

Since the electric field strength is higher near the electrodes, NWs will experience a DEP force towards the electrodes, as demonstrated in Figure 2.6(b). The force magnitude depends on the square of the gradient of the electric field strength. The NWs dragged to the electrodes serve as anchors for other NWs to bridge across the electrode gaps. The DEP forces should be strong enough so that NW chains will not be disrupted by other forces, such as Brownian motion. However, if DEP forces are too strong, too many NWs will be dragged to the region near the electrodes and not enough NWs will be left to bridge electrode gaps.

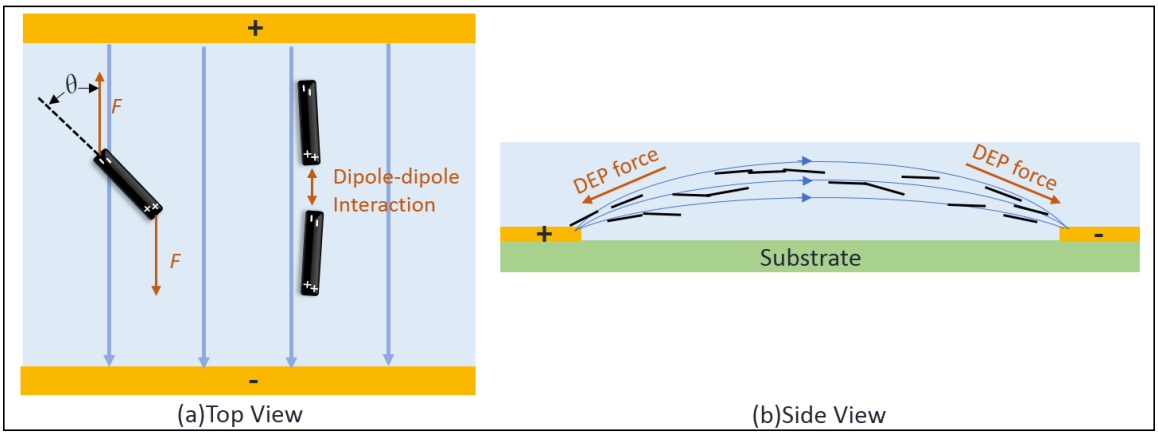

Figure 2.6 Sketch of forces experienced by NWs in an electric field from (a) top view and (b) side view.

In addition, NWs in the electric field have an induced dipole moment, and the dipole moment causes torque on the NWs [42]. The torque tends to align the long axis of the NW with the direction of the electric field as shown in the left sketch in Figure 2.6 (a). When a NW aligns parallel to the electric field, its dipole has lower potential energy than when it is at an angle with the field. The alignment torque scales in proportion to the square of the electric field strength [43].

Apart from the translational motion and rotational motion of the NWs from interaction with the electric field, NWs also interacts with each other. The different dipoles on NWs attract each other, as shown in the right sketch in Figure 2.6(a), and connect the NWs into chains. Dipole-dipole interaction plays an important role in the region far away from the electrode, where the electric field gradient is weak [13].

2.2.2 Disruptors in NW chaining

There are a few physical mechanisms that could stop the NW chaining process or damage the NW chains formed during the process. The main disruptors include electrical double layer (EDL), electroosmotic flow, capillary forces and Brownian motion. The effects of these disruptors can be reduced by choosing parameter values, or by having the directed effects overcome them.

Electrical double layer (EDL)

EDL is a structure formed on the surface of an object when it is in contact with fluid. In NW chaining process, the EDL can form on the NWs as well as the electrodes. As implied in the name, EDL has two layers. The first layer is called the surface charge layer, which is made of ions or polar molecules tightly anchored on the object surface. The second layer consists of ions or polar molecules that are attracted to the first layer by Coulomb force, which is loosely associated with the object [44]. The thickness of EDL is described by the reciprocal Debye length [44]:

$$\kappa^{-1} = \sqrt{\frac{\varepsilon_m \varepsilon_0 k_B T}{\sum_i e^2 z_i^2 n_i}}, \tag{3}$$

in which ε_0 is the permittivity of free space; k_B is the Boltzmann constant; T is temperature; e is the elementary charge for a single electron or proton; z is the ionic valence, and n is the ionic concentration. EDL is one of the disruptors in the NW chaining process. When an EDL appears above the electrodes, it behaves like a capacitance, which could reduce the voltage imposed on the NW suspension. EDLs also could occur at the polarized ends of NWs, which reduces or eliminates the directed effects of the electric field. Therefore, the frequency of the applied AC field is required to be higher than the relaxation frequency of the ions and polar molecules in the NW suspension to supress this disruptor [11].

Electroosmotic flow

Electroosmotic flow appears when the surface charges in the EDL interact with the electric field, causing a vortical motion of the fluid [45], as demonstrated in Figure 2.7. The vortical flow can prevent NWs from settling down in chains or destroy NWs chains formed in the chaining process. Therefore, electroosmotic flow is a potentially strong disruptor for NW chaining. The driving force of this flow is called electroosmotic force: $F = qE_t$, in which q is the surface charge density and E_t is the tangential field strength.

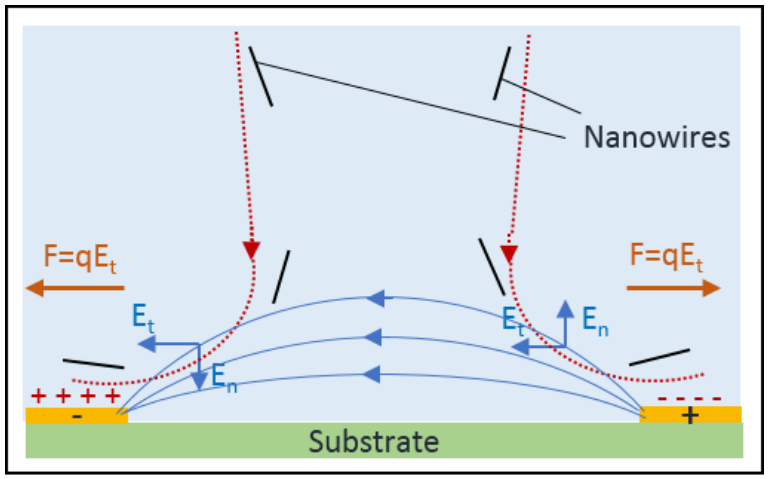

Figure 2.7 Schematic drawing of the electroosmotic flow. Drawing inspired by [46]**.**

The velocity of electroosmotic flow, v, can be calculated by [47]:

$$v = \frac{\varepsilon_m {V_{rms}}^2}{4x\eta} \frac{\Omega^2}{(1+\Omega^2)^2}, \tag{4}$$

where V_{rms} is the applied voltage, x is the characteristic length, half of the gap size in our case, η is the dynamic viscosity of the electrolyte, and Ω is a dimensionless frequency defined as:

$$\Omega = \frac{\pi}{2} x\kappa\omega \left(\frac{\varepsilon_m}{\sigma_m}\right), \tag{5}$$

in which κ is the reciprocal Debye length of the EDL; x is the characteristic length, which is half of the gap size between electrodes, and σ_m is the electrical conductivity of the medium. Thus, the velocity of electroosmotic flow depends on the thickness of EDL. Electroosmotic flow and EDL are coupled disruptors. Sam et al. [46] have built a framework to minimize the electroosmotic flow. It was found that at high enough frequencies the electroosmotic force is small because the EDL does not have enough time to develop. 10kHz was found by calculations and experiments to be an appropriate frequency to minimize the electroosmotic flow for NW chaining [13].

Brownian motion tends to randomize the orientation and position of NWs. Therefore, it can be disruptive if it is comparable to or larger than DEP forces. The extent of competition

between Brownian motion and DEP forces for the NWs can be described by the ratio of Brownian to DEP displacement. This ratio has been estimated for spherical particles [48] and cylindrical NWs [11]. M. Sam has calculated this ratio to be about 0.05 under the NW chaining experimental conditions [11], which indicates that the effect of DEP forces is significantly stronger that the effect of Brownian motion. Observations during NW chaining experiments also show that Brownian motion is not a predominant disrupter.

Capillary force can be disruptive in two ways: spreading the NW suspension to undesirable areas, and pulling away NWs at the drying fronts [49]. In order to control the NW suspension in the desired area, a dam with several channels was introduced [13], which is shown in Figure 2.11. Using the dam also prevents rapid dryout of the alcohol and gives excess time for the NW chains to form and the DEP forces to secure NW chain ends within the wells.

2.3 Fabrication

2.3.1 Ag NWs

The Ag NWs used in this research were bought from Sigma Aldrich; they come as suspension in IPA. The original concentration was 3.9mg/mL, and it was diluted into different concentrations for experiments. Figure 2.8 shows a picture of Ag NW suspension after dilution. The NWs have average length and diameter of 35μm and 115nm, respectively. They were synthesized by polyol method. This section provides a brief literature review of Ag NW synthesis.

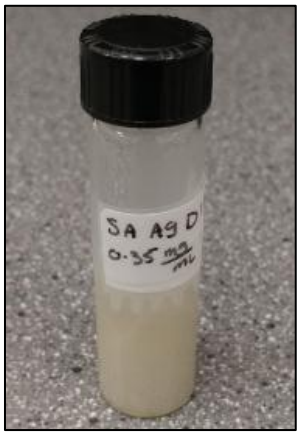

Figure 2.8 Diluted Ag NW suspension with a concentration of 0.35mg/mL

Ag NWs can be synthesized by several methods, which can be categorized into template-directed and template-free methods. Template-directed synthesis deposits Ag in nanoscale channels by electrochemical or chemical approaches, and thus controls morphology of the Ag NWs. The main limitation of template-directed synthesis is high cost and difficulty to scale up [50]. In contrast, template-free methods can synthesize Ag NWs in solution and are easy to scale up. In the template-free category, the polyol method has been used widely because of its simplicity, high yield, and cost effectiveness [51].

In the polyol method, a solution of ethylene glycol (EG), silver nitrate, and poly(vinyl pyrrolidone) (PVP) are heated. EG is the polyol solvent and reducing agent. Silver ions are chemically reduced in the presence of PVP, which serves as a capping agent. The polyol method could be processed by added seeds, or self-seeding [52]. The PVP interacts with {100} facets and passivates them, which directs Ag addition onto the {111} facets and thus the structures grow in one direction to form NWs [53]. The growth of Ag NWs by polyol method is demonstrated in Figure 2.9. The PVP is an essential material in synthesis of Ag NWs by polyol method, but the PVP residue strongly affect the electrical conductivity of TEs made by Ag NWs, which requires post-treatments, and will be discussed in Chapter 3.

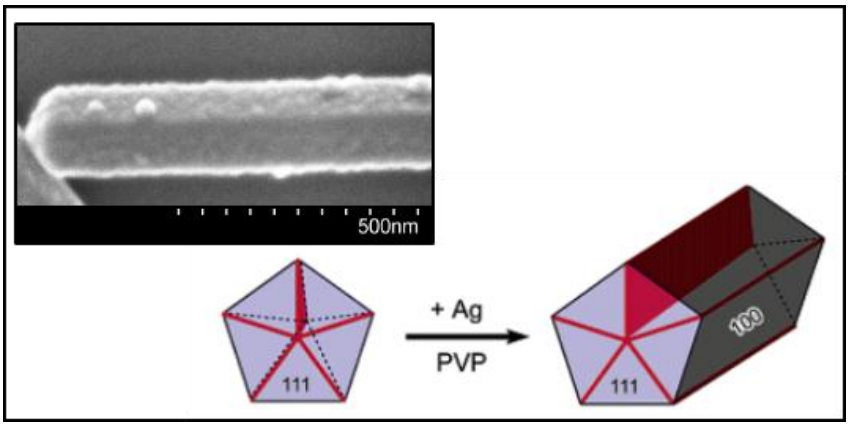

Figure 2.9 Schematic illustration of an Ag NW growth by polyol method. The cross section of the NW is pentagonal shape; the side surfaces are {100} facets, and the two ends are formed by {111} facets. Picture taken from [53]**. A SEM image of NW shape is inserted at the top left corner.**

2.3.2 Interdigitated electrode substrates

The electric field is applied to the NW suspension through interdigitated electrodes. The interdigitated electrodes are gold patterns created on glass or silicon wafer using photolithography, followed by lift-off process. A mask was required in photolithography. The mask was first designed using a software, L-Edit, and then produced by a mask writer [12]. The void area in a mask ended up corresponding gold pattern on the substrates. The procedures of photolithography and lift-off process were modified from Sahar. M's work [11], and the details are presented in Procedures of photolithography and lift-off process.

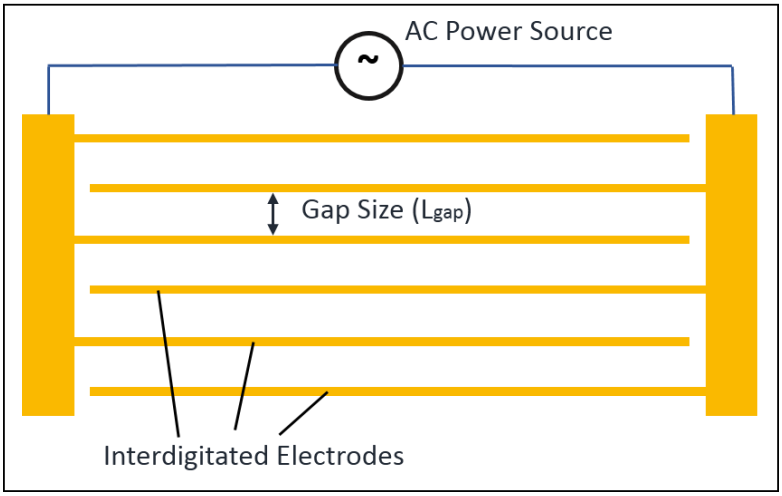

Figure 2.10 Schematic of interdigitated electrodes

The gold pattern of interdigitated electrodes is illustrated in Figure 2.10. Each set of interdigitated electrodes are connected to a set of gold pads, through which the AC power source is connected to. Assuming the resistance of the gold pattern is negligible, then all the electrodes that connect to the same big gold pad will have the same electrical potential. The thickness of the gold pattern is 50nm. Experiments have shown that any thickness of no less than 8nm will result in functional electrodes in NW chaining. The width and length of each interdigitated electrode are 30μm and 20mm, respectively. The distance between two interdigitated electrodes is defined as the gap size, L_{gap}. The gap sizes used in this research are 120μm, 180μm, 240μm, 300μm, 360μm and 420μm. The effective area of the substrate is about 12mm×20mm, and the number of interdigitated electrodes varies according to the gap size. For example, with a gap size 120μm, the number of interdigitated electrodes is 78.

2.3.3 Experiment setup and process

NW chaining can be done directly on a rigid substrate with patterned interdigitated electrodes, but on a polymer spun on the substrate. The experiment setup and process for a rigid substrate and polymer is the same, other than the applied voltage and frequency. This is because polymers coated on conductive films behave like capacitors [54]. Capacitors have high impedance at low frequencies and will over divide the voltage from the source. The NW suspension will then have a low voltage imposed on it, and the electric field will

be weakened. Therefore, NW chaining on polymer requires a higher frequency and voltage than on the rigid substrate. Since this thesis mainly focuses on ordered NW networks on polymer, the methods of NW chaining on polymer is introduced here.

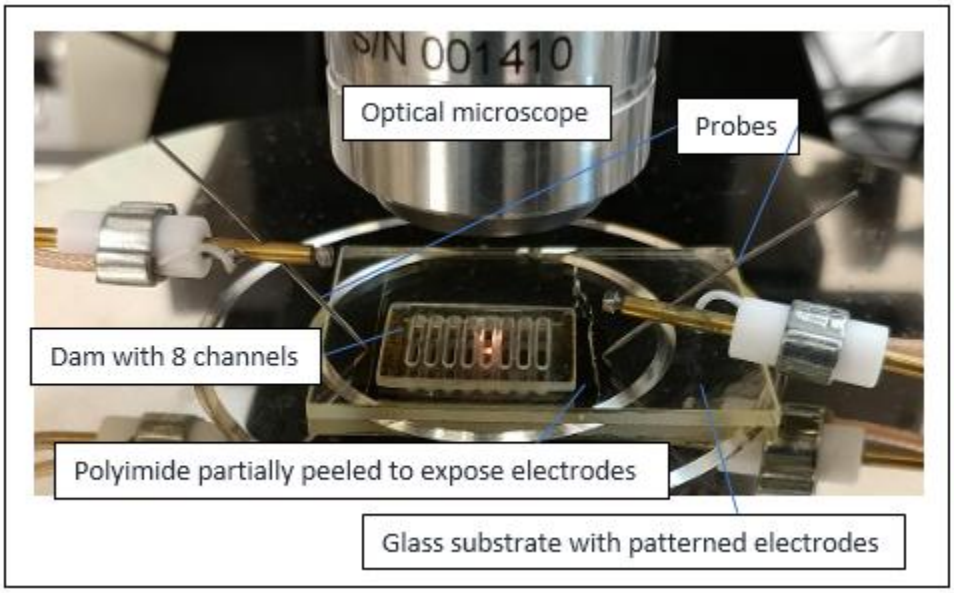

Figure 2.11 Experiment setup for NW chaining on polymer substrate

On a rigid substrate with patterned interdigitated electrodes, a layer of polyimide (VTEC 1388) is spun and baked. At a spin coating speed of 3500rpm, the polyimide thickness is measured to be about 7μm by a Bruker profilometer model DekTak XT. Figure 2.11 shows the experiment setup of NW chaining. The polyimide is partially at the position of electrodes to allow the contact probe tips and the electrodes to apply voltage. A dam with channels is placed on the polymer. The dam channels define the location of ordered NW networks and moderate the motion of the alcohol drying front to prevent NW chain destruction. $7V_{rms}$ voltage with 100kHz frequency is applied. With the electric field on, NW suspension is added to the channels. Directed by the electric field, NWs connect into chains. As the alcohol dries out, NWs settle down on the polymer as ordered NW networks.

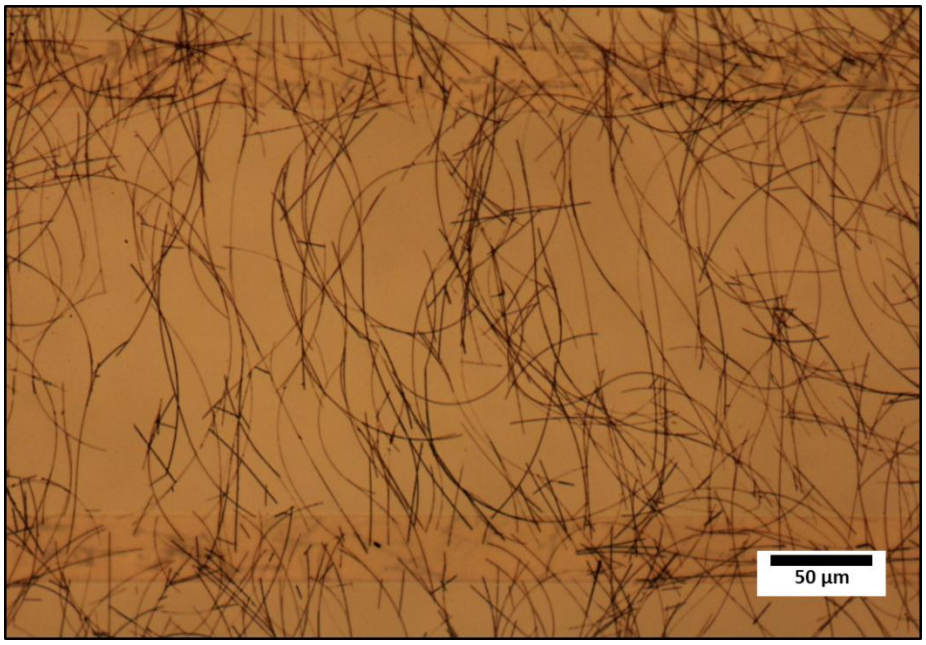

Figure 2.12 A micrograph of ordered NW networks on polyimide substrate. The gap size between the two electrodes is 180µm. The NW concentration was 0.25 mg/mL.

Figure 2.12 shows an example of ordered NW networks created on the polymer. To demonstrate the difference made by the electric field, the same experiment was repeated but without applying the electric field. The resulting random NW networks is shown in Figure F.1. The electric field not only aligned and connected the NWs, but also made the NWs distribute more evenly over the polymer substrate. However, there is one NW connection problem in the resulting ordered NW networks; it is difficult to form NW chains directly over the interdigitated electrodes. The problem is caused by the weaker directors for NW chaining in this region, which will be further explained by field distributions from simulations in Chapter 4. It should be possible to fix the problem by a second step of NW chaining to bridge this region; electrodes for NW chaining in the second step need to be designed.

The polymer with NW networks can be peeled off from the rigid substrate. The van der Waals force between NWs and the polymer is strong enough to keep the NWs in their positions and thus maintain the NW chain configuration. After peeling off the polymer, the patterned rigid substrate can be reused.

2.4 Characterization

2.4.1 Transparency

When light hits an object, it is reflected, transmitted, or absorbed. Light transmittance of a material measures its capacity to transmit light through itself, and is defined by the ratio of the transmitted light to the incident light. Light transmittance of a material varies with different wavelengths. Since solar spectrum has the highest intensity at roughly 550nm wavelength, most researchers of transparent electrodes report the transparency at 550nm wavelength of their samples [55]. Since the transmittance of NW networks highly depends on the percentage of area that is covered by NWs, they have similar transmittance from the wavelength of 380nm to 800nm. Therefore, transmittances at 550nm wavelength were taken as the transparency of the NW networks in this research.

The transparency measurement in this work was done by a Cary 50 UV-Vis spectrophotometer. This spectrophotometer uses a dual light beam to measure the light transmittance. A schematic of how this spectrophotometer measures light transmittance is shown in Figure 2.13. A light beam from the light source is first split equally into two beams, with the intensity of I_0. One beam enters the silicon diode detector, which measures the intensity. The other beam passes through the sample and enters another silicon diode detector, which measure the intensity of transmitted light, I [56]. The corresponding software then calculates the transmittance of the sample using this equation:

$$\%T = \frac{I}{I_0} \tag{6}$$

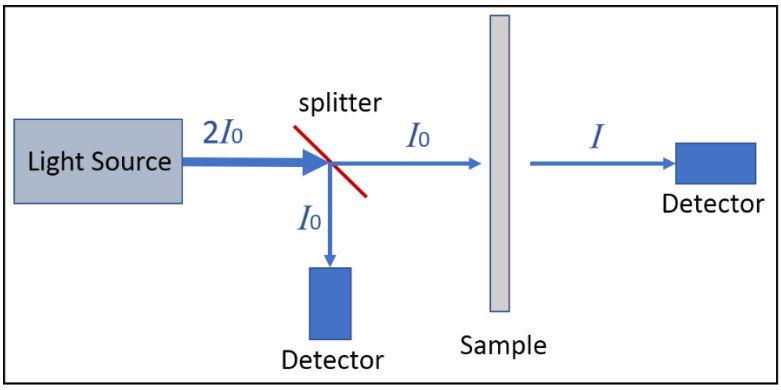

Figure 2.13 Illustration of how the spectrophotometer measures light transmittance using a dual light beam

The light beam of this spectrophotometer is in a rectangular shape, with a height of 1.13 mm and a width of 0.71 mm. The smallest dimension of our ordered NW networks samples is 1mm, which makes it possible that the whole light beam passes through the sample. The measuring error of this spectrophotometer is not reported in its specification sheet, but our colleague Jehad Alsaif tested it to be ±1.5% when measuring NW networks [12].

Transmitted light includes specular light and diffusive light. Specular light is the transmitted light that continues in the direction of incident light. Specular light makes the object look transparent. Diffusive light is the transmitted light that is scattered by the object, which make the object look hazy. Only the specular light is measured in this research. The light transmittance of NW networks reported in this thesis use the substrates as references, i.e. for NW networks on polyimide, the polyimide with the interdigitated electrodes on glass is used as a reference, and for NW networks on PET, the PET sheet is used as a reference. The transparency of ordered NW networks on polyimide decreases with the increase of the NW suspensions. For NWs concentrations of 0.25, 0.35, and 0.45mg/mL on polyimide substrate with a thickness of 7μm, the transparency are 95.4%, 94.0%, and 92.3%, respectively.

2.4.2 Sheet resistance

Resistivity (ρ) is a physical property to represent a material's ability to conduct electricity. The relationship between resistance and resistivity is:

$$R = \rho \frac{L}{A} \tag{7}$$

Where L is the length of the object and A is the cross-sectional area, which is $W \times t$ in the case of thin film; W and t are the width and thickness of the thin film respectively. To report and compare the resistivity of thin films, it requires measurement of thickness. Since sometimes the thickness of thin films is hard to measure accurately, the resistance per square area is used to represent the conductivity instead of resistivity. The resistance per square area is called sheet resistance (R_s), with its unit as Ohm/square (Ω/sq). Figure 2.14 demonstrates how to achieve the sheet resistance of a rectangular shape thin film. If the dimension of thin film in the direction of current is L, and the other dimension is W, then the number of squares is L/W. If the resistance is measured as R, then the resistance per square can be calculated by:

$$R_s = \frac{R}{(\frac{L}{W})} = R \frac{W}{L} \tag{8}$$

Rearranging equations (7) and (8) results in the relationship between resistivity and sheet resistance:

$$R_s = \frac{\rho}{t} \tag{9}$$

Note that sheet resistance is related to the resistivity and thickness, and not related to the size of the square. Therefore, the size of square chosen in the measurement and calculation would not affect the result of sheet resistance. The sheet resistance reported in this thesis is calculated using equation (8).

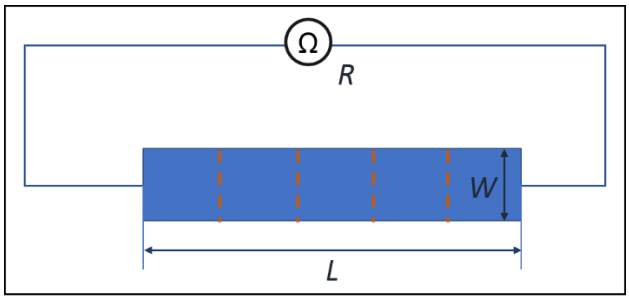

Figure 2.14 Illustration of sheet resistance measurement of a rectangular shape thin film

The resistance measurement in this thesis was done by a Keithley 6340 source meter using 4-point mode, which is available with the 4-point probe station. The reason to use 4-point measurement is that the result will be more accurate than a regular 2-point measurement. In a 2-point measurement, the two probes are supplying the current and sensing the voltage at the same time. Both the resistance of the leads and the contact resistance between the probes and the sample are in series with the sample resistance, resulting in higher resistance than the actual value. In a 4-point measurement, supplying current and sensing voltage are conducted separately by two pairs of probes. In addition, the current supply probes are placed further out than the voltage sensing probes, so that the contribution of the contact resistance would be eliminated [57].

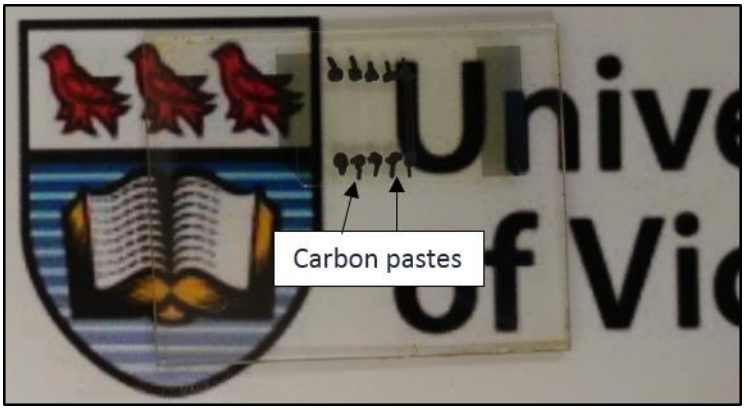

Figure 2.15 Fabricated TEs with ordered Ag NW networks. Carbon paste were applied to both ends of every TE, enabling resistance measurement.

An example of fabricated ordered NW networks is demonstrated in Figure 2.15. Carbon paste was introduced to contact the probes in resistance measurement. The sheet resistance of ordered NW networks depends on post-treatments, and NW concentrations. Ordered

NW networks before post-treatment show a sheet resistance of 10~200 kΩ/sq, and post-treatments can improve it to 20~30 Ω/sq, depending on the NW concentration. The detailed method of post-treatments will be presented in Chapter 3. Without applying the electric field, NW networks created by the same experiment procedures show a sheet resistance of 0.5-200 kΩ/sq after post-treatment.

2.4.3 Figure of Merit (FOM)

TE applications require optimization of electrical and optical properties. Based on the specific device, minimum values for electrical conductivity and transparency of TE must be met. Generally, the higher that both properties are, the better [55]. However, among ITO and its alternatives, higher electrical conductivity results in lower transparency, and vice versa. Therefore, some FOMs are needed to determine which combination of electrical conductivity and transparency is optimal. There are two FOMs widely used in TE researches, the electrical to optical conductivity ratio (σ_{DC}/σ_{OP}) [36] [58], and Haacke's FOM (φ_H) [55] [37]. The higher values of FOMs represent the better the performance of electrical conductivity and transparency. In this work, Haacke's FOM is chosen to compare the performance of TEs. The following part will introduce these two FOMs and explain why Haacke's FOM was chosen in this research.

The electrical to optical conductivity ratio, σ_{DC}/σ_{OP}, is usually used to describe performance of traditional transparent conductors, and bulk-like films. The relationship between transmittance and sheet resistance of these type of materials can be expressed in this equation [59]:

$$\%T = [1 + \frac{Z_0}{2R_s}\frac{\sigma_{OP}}{\sigma_{DC}}]^{-2} \quad (10)$$

Where σ_{OP} is the optical conductivity of the material, σ_{DC} is the bulk DC conductivity of the film, and Z_0 is the impedance of free space, with its value as 377Ω, thus the corresponding value of $\frac{Z_0}{2}$ is 188.5Ω. Rearranging equation (10), and the FOM σ_{DC}/σ_{OP} can be expressed with R_s and $\%T$ in the following equation:

$$\frac{\sigma_{DC}}{\sigma_{OP}} = \frac{188.5\Omega}{R_s(\%T^{-\frac{1}{2}} - 1)} \tag{11}$$

This FOM is used for thin and uniform transparent conductors, and its value is dependent on the film thickness. Coleman et.al. [60] reported that nanowire and nanotube films below a critical thickness behaves differently from the bulk-like properties described in equation (10). The reason for the deviation may be the non-uniformity and the percolation effects (connected materials) in the very thin film of NWs and nanotubes.

A common used FOM for comparing TE performance was proposed by Haacke [55]. The definition of Haacke's FOM is:

$$\varphi_H = \frac{\%T^{10}}{R_s} \tag{12}$$

Its unit is Ω^{-1}. The exponent 10 for $\%T$ has been chosen because it makes the maximum FOM of a transparent conductor film occur when the transparency is 90%, which is also the transparency benchmark of ITO. In addition, the exponent 10 simplifies the numerical calculations for FOM, which makes it a favorable choice in practical application. Haacke has detailed technical discussion of how this FOM was shaped [55], which is summarised in Appendix A for the further understanding or interest of the readers. Since the TEs reported in this thesis are made of NWs and their thickness is not uniform, σ_{DC}/σ_{OP} would not be an appropriate measurement for performance. Therefore, Haacke's FOM was chosen for measuring and comparing the TEs in this work. Unless specifically stated, the FOM values in the rest of this thesis are based on Haacke's FOM.

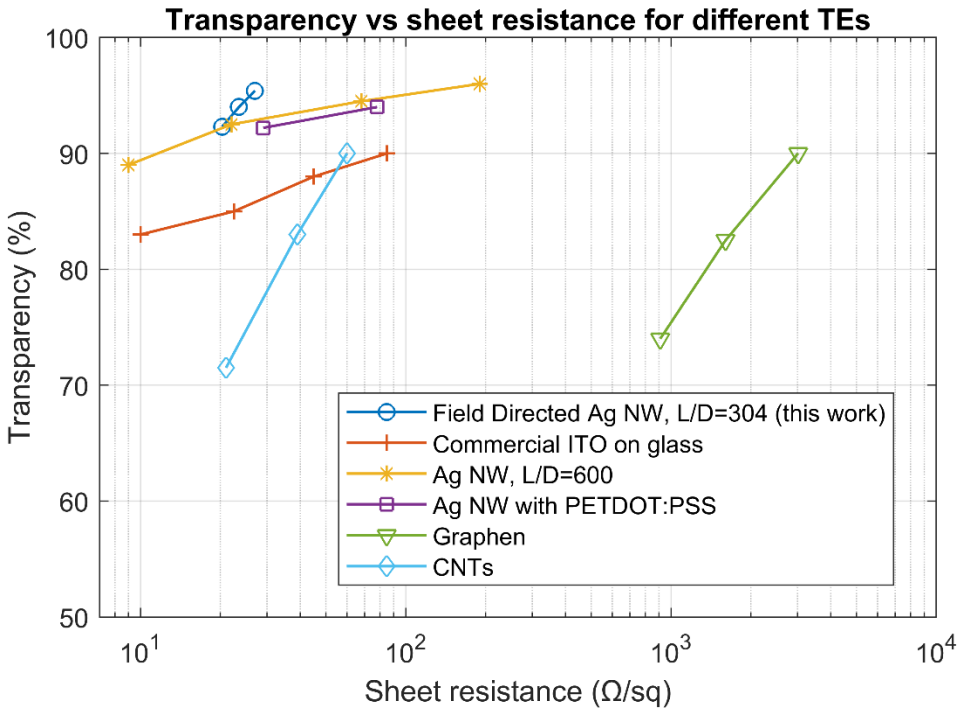

Figure 2.16 Comparison of transparency and sheet resistance among the best available TEs, including this work, commercial ITO [61]**, very long Ag NW networks** [62]**, Ag NW with PETDOT:PSS** [37]**, graphene** [63]**, CNT networks** [19]**.**

The best FOM shown in ordered NW network in this research is $0.023\Omega^{-1}$. In contrast, commercially available ITO with 70nm coating on glass has the sheet resistance of about 70Ω/sq and transparency of 90%; its FOM is $0.005\Omega^{-1}$ [64][61]. As introduced at the beginning of this chapter, there are several types of ITO alternatives being sought. Figure 2.16 compares the transparency and sheet resistance of some of the high-performance TEs reported in the literature. In this graph, the data points that fall closer to the left and top corner indicate higher performance. The comparison shows that the performance of ordered NW networks is very competitive among ITO alternatives and outperforms commercial ITO.

2.4.4 Cost

The main cost of ordered NW networks in this research comes from two sources, the Ag NWs and fabrication of substrate with interdigitated electrodes. Ag is an expensive material, about 17.2 USD/oz, according to US Geological Survey [65]. According to this

price, the Ag used to fabricate $1m^2$ of ordered NW networks with sheet resistance of 27 Ω/sq and 95.4% transparency costs only 0.05 CAD. However, the price of Ag NW suspension is much higher than the Ag it contains. The Ag NW suspension used in this research was purchased from Sigma Aldrich at 360 CAD for 25mL at 3.9mg/mL concentration. Based on this price, the Ag NW suspension used in ordered NW networks with the same performance is $231CAD/m^2$. With the fabrication tools available at UVic, it costs about 150CAD of materials and tools access to make 6 substrates, of which each has $4320mm^2$ effective area. However, after fabrication of ordered NW networks, the polyimide with NW networks can be peeled off from the substrates and the substrates can be reused again and again. Therefore, the cost of substrates depends on how many times the substrates are used, and it can be very low if they are reused a large number of times. In comparison, commercial ITO with sheet resistance of 30-60Ω/sq and 84% transparency at 550nm costs 115CAD for $625mm^2$ area, according to Sigma Aldrich quote [66]; the price is equivalent to $184kCAD/mm^2$. Therefore, ordered NW networks potentially have a much lower cost than ITO.

2.5 Mathematical models for ordered NW networks

Transparency and sheet resistance are the two key quantity parameters of transparent electrodes. When the NW concentration increases, both sheet resistance and transmittance decrease, and vice versa. Post-treatment can improve the conductivity of NW-NW junctions and reduce sheet resistance. However, no matter how much the junction contact resistance can be lowered by post-treatment, there is a limit to the performance, which is regulated by the morphology of the NW network. It is shown that ordered NW networks perform better than disordered networks, but no matter how ordered the NW network can be, there is a limit to the performance, set by the size and resistivity of the NWs. What would the limit be? What would the relationship between the transparency and sheet resistance be when the limit is reached? And how would their relationship change in a practical scenario?

2.5.1 Percolation theory for random NW networks

For a NW network to be electrically conductive, a current must be able to pass across it. In a NW network, charge carriers travel along the NW length and change direction from one NW to another at the junction. Therefore, the connectivity of NWs across the network is crucial. Percolation theory studies the connectivity of NWs over the random NW networks, and the effects of network density on the conductivity of the NW networks.

The network density, *N*, is defined as the number of NW per unit area, which is an important parameter in percolation theory. If NWs are added on a flat surface between two electrodes, at some point the first continuous path is formed by NWs, and the NW network achieves percolation. The network density at this point is defined as critical network density, N_c. The N_c for random networks was achieved by GE Pike and CH Seager, using Monte Carlo simulations, assuming NWs are widthless sticks distributed randomly on a 2D plane. The critical network density depends on the length of NWs, *L*, which is shown in the following equation [67]:

$$N_c L^2 = 5.71\,. \tag{13}$$

Note that it was found later that 5.637 is a more accurate number than 5.71 in the equation [68]. The equation indicates the benefit of using long NWs, because the critical network density would decrease to one fourth of its original value if the NW length is doubled.

After the critical network density is reached, if more NWs are added to the network, the NW network will become more conductive, because more NWs will be connected into the conducting path. The conductivity of the NW network, σ, is defined as the inverse of sheet resistance. The following equation describes how σ will change with the network density *N*, after percolation is achieved [69]:

$$\sigma \propto (N - N_c)^t \tag{14}$$

The exponent *t* in the equation is called conductivity exponent, which is determined by the spatial geometry of the network. For a 2D network, the value of *t* is 1.33. However, NW networks are not perfect 2D networks. When charge carriers travel from one NW to another

at the junction, they are out of the 2D plane. Experimental data have fitting curves showing the value of t varies from 1.42 to 1.5 for Ag NW networks [70]. Experimental data have shown that percolation theory also fits well with networks made of CNTs, with *t* ranging from 1.46 to 1.65 [71].

Although percolation theory is proven to be effective to describe random NW networks, there are a few limitations. Firstly, percolation theory has not considered the effect of junction resistance, which is shown in literature to be much larger than the resistance of the NWs [38]. Secondly, the theory is based on the average length of NWs, and a wide range distribution of NW lengths may affect the results [67]. Finally, the theory is designed for random NW networks, but in real fabrication, total randomness is difficult to achieve, and it can not be used for ordered NW networks. Therefore, a model designed for ordered NW networks is needed.

2.5.2 Model 1: Ideal NW chains model

The ideal NW chains model gives an upper bound limit of the NW network performance, and the relationship between transmittance and sheet resistance. In this model, the morphology of the NW networks is optimized as perfectly straight NW chains, and NW junctions are ideally connected so that they are as conductive as the NWs themselves. This situation is the best scenario for the performance of NW networks for a given type of NWs.

Careful consideration of assumptions, parameters, and calculations is required. These are the assumption for the model: All NWs have the same shape, are perfectly formed into end-to-end chains, are orientated in the direction of the electric field, and their junctions are welded perfectly by post-treatments so that their resistance is negligible. Parameters in the model includes: NW length and diameter are L and D respectively; the conductivity of the NW is ρ; the number of the NWs is n; NWs are deposited on a square substrate which length is a. The following calculations were used to evaluate the performance of ordered NW networks. The number of NWs needed to build the first ideal chains is $n_c = a/L$; if there are just enough NWs to build p chains, then $n = p \cdot n_c$, $(p \in N)$; the resistance of one NW is:

$$R_{NW} = \rho \frac{L}{\mathrm{A}} = \frac{4\rho L}{\pi D^2}. \quad (15)$$

The resistance of one chain is $R_c = n_c \cdot R_{NW}$; Since it is on a square substrate, the sheet resistance is equal to the total resistance:

$$R_s = \frac{n_c}{n} \cdot R_c = \frac{4\rho a^2}{\pi n D^2 L}. \quad (16)$$

The area blocked by one NW is *DL*, and there is no overlap NW in this model, so the total area blocked by the NWs is *nDL* and the transmittance of the substrate is:

$$\%T = 1 - \frac{nDL}{a^2}. \quad (17)$$

Rearranging the equations, we get the relationship between the transmittance and sheet resistance:

$$\%T = 1 - \frac{1}{R_s} \cdot \frac{4\rho}{\pi D}. \quad (18)$$

This equation predicts the upper bound of NW networks when the Ag NWs in our experiments are used. In conclusion, there is a linear relationship between the transmittance and inverse sheet resistance of perfectly aligned and welded NW chains.

2.5.3 Model 2: NW chains model for practical scenarios

Model 2 considers the fact that it is challenging to fabricate a strictly ordered NW network, so as to perfectly weld the NW junctions. Therefore, the assumptions are adjusted, and several factors are introduced to describe the imperfect extension of NW network morphology and NW junction conductivity.

The assumptions were modified, imperfect factors were introduced, and calculations were revised. These are the assumptions: All NWs have the same cylindrical shape; a portion of NWs is formed into end-to-end chains; on average, one NW contacts other NWs twice. Three factors were introduced to describe the imperfect extension of NW networks: The ratio of a contact resistance to a NW resistance is k_1, $k_1 > 0$; the length of each NW chain is k_2 times the length in the ideal model, $k_2 > 1$; k_3 is the functional NWs ratio, $1 > k_3 > 0$.

Calculations were revised in the following manner: The number of NWs needed to build the first perfect chains is $n_c = \frac{a}{L} \cdot k_2$; if just enough NWs to build *p* chains, then $n \cdot k_3 = p \cdot n_c$, $(p \in N)$. The contact resistance of a NW junction: $R_{jun} = k_1 \cdot R_{NW}$; the resistance of one chain is

$$R_c = n_c \cdot R_{NW} \cdot (1 + k_1). \tag{19}$$

Since it is on a square substrate, the sheet resistance is equal to the total resistance:

$$R_s = \frac{n_c}{n \cdot k_3} \cdot R_c = \frac{4\rho a^2}{\pi n D^2 L} \cdot \frac{(k_1 + 1) \cdot {k_2}^2}{k_3}. \tag{20}$$

The area blocked by one single NW is *DL*, but NW overlapping should be taken into consideration for calculations of transparency in this model. Based on the assumption that, on average, one NW makes contact twice with other NWs, we need to subtract a D^2 from the blocking area for each NW. As a result, the total area blocked by the NWs is *nD(L-D)*; the transmittance of the substrate is:

$$\%T = 1 - \frac{nDL}{a^2} \cdot \left(1 - \frac{D}{L}\right). \tag{21}$$

Rearranging the equations, we get the relationship between the transmittance and sheet resistance:

$$\%T = 1 - \frac{1}{R_s} \cdot \frac{4\rho}{\pi D} \cdot \left(1 - \frac{D}{L}\right) \cdot \frac{(k_1 + 1) \cdot {k_2}^2}{k_3}. \tag{22}$$

2.6 Conclusions

This chapter introduces the NW chaining technique established in our laboratory for fabricating ordered NW networks. Substrates with well-defined parallel electrodes were fabricated by photolithography for applying an AC electric field over the NW suspension. NWs are connected into chains by DEP force and dipole-dipole interaction from suspension. FOM measures the overall optical and electrical properties of TEs. Ordered

NW networks on polyimide by this technique show a FOM of 0.023Ω-1, which is competitive among ITO alternatives reported and higher than the FOM of commercial ITO, 0.005Ω-1. The cost of ordered NW networks is estimated to be much lower than ITO, and would be maintained at a low cost in large area production, since they are processed from solution. An ideal NW chain model was built, and it shows a linear relationship between transparency and inverse sheet resistance. Imperfect factors were considered to modify the model for practical scenarios.

Chapter 3 Joule heating to improve conductivity of ordered Ag NW networks

As stated in Chapter 2, PVP is essential for Ag NWs synthesised by the polyol method. However, the surfactant coating of PVP of Ag NWs results in the high resistance at NW-NW junctions [19]. In our experiment, ordered NW networks, without any post-treatment, typically have a sheet resistance of around 10~200 kΩ/sq. Post-treatment is necessary to improve the conductivity of Ag NW networks or chains and reduces this resistance by several orders of magnitude, making it competitive with ITO. In this chapter, Joule heating, which employs an electric current to generate heat, is investigated to weld NW-NW junctions and improve the conductivity of ordered Ag NW networks.

3.1 Post-treatments and Joule heating

The main source of resistance in Ag NW networks comes from the NW-NW junctions. Ag NWs have very high electrical conductivity along the direction of their length. NW-NW junctions have high resistance because of the smaller contact area compared to the cross section of the NWs and the added contact resistance of the nonconductive PVP residue. The initial resistance of a single Ag NW junction was measured and reported to be between 1×10^{12} and $1\times10^{14}\Omega$ [1], while the resistance of a Ag NW with 115nm diameter and 35μm length (average Ag NW size used in this research) is about 54Ω.

Researchers have used a variety of post-treatments to improve the junction contacts and thus increase the conductivity of Ag NW networks, such as thermal annealing [72] [26], mechanical pressing [73] , laser welding [74], plasmonic welding [75], and Joule heating [76]. Among these methods, we may expect Joule heating to show significantly different behaviour between random NW networks and our more ordered chained NW networks. This is because the heating current path is determined by the number, distribution and evolving resistance of NW junctions. Since NW-junction resistance is significantly higher than NW resistance, heat generation occurs predominantly at the junctions. In ordered networks, these occupy a smaller fraction of the total NW-chained area, reducing damage to temperature sensitive substrates such as polymer.

3.2 Joule heating calculations on ordered NW networks VS random NW networks

Joule heating is performed by running a current through NW networks and generating heat. This is noticed particularly at the NW junctions. Its effect is heavily influenced by the current distribution and path. Ordered NW networks in this work and random NW networks have different NW configurations; the former have more NW connected in chain sequence while the latter have more NW connected into branches. Due to the different geometries, the current distribution and heat generation could have different behaviors during Joule heating.

In order to study the difference between Joule heating in ordered NW networks and random NW networks, we studied current and power distribution using Matlab Simulink. Since NW-NW junctions have much higher resistance than the NWs themselves, the resistance of NWs is omitted in this study. Models for straight-chain and branched resistors are shown in Figure 3.1 and Figure 3.2, respectively. A DC current is applied to the networks in both cases. Simulink can calculate the current passing through each resistor.

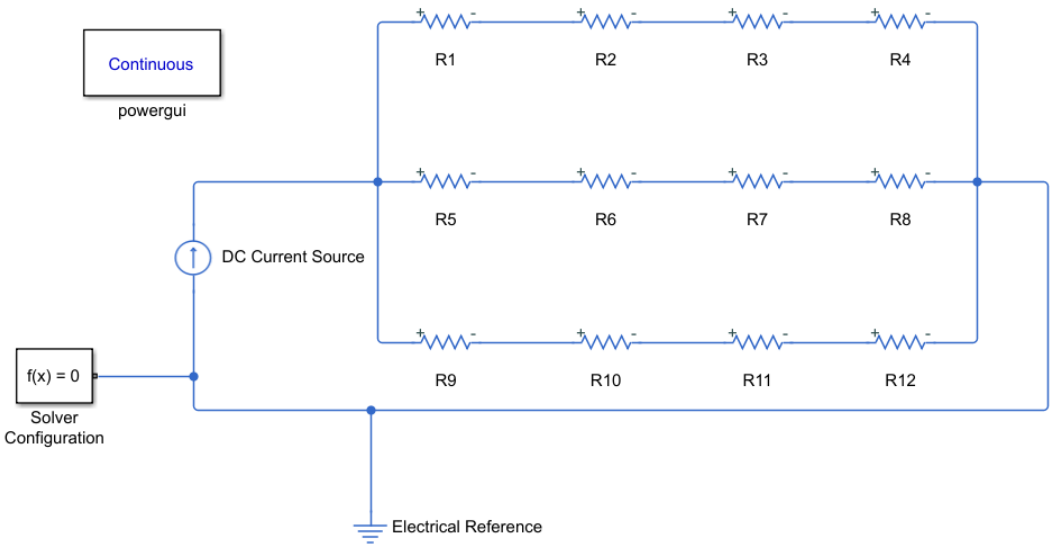

Figure 3.1 Joule heating setup of chained networks in Simulink

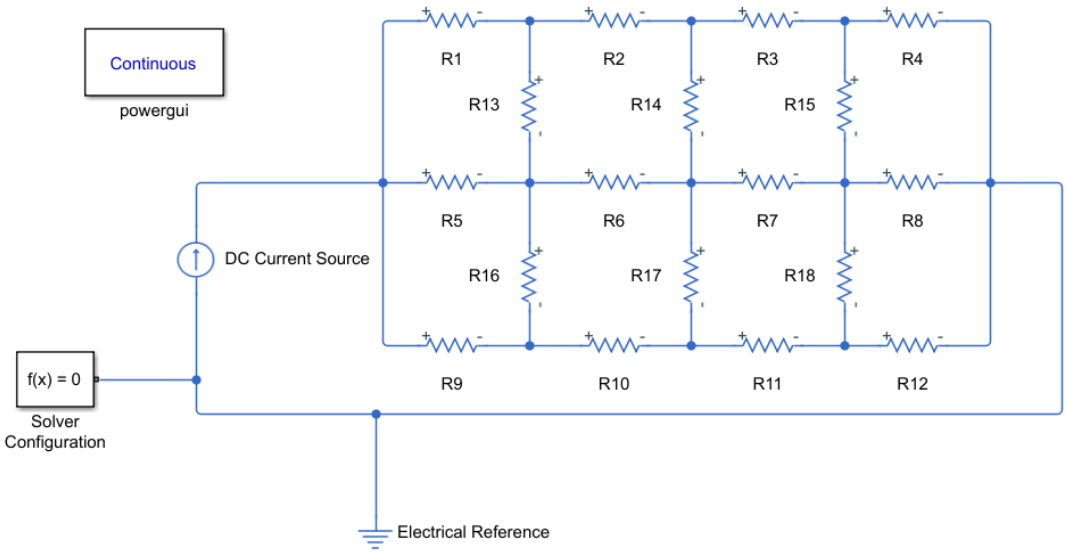

Figure 3.2 Joule heating setup of branched networks in Simulink

3.2.1 Results and discussion

When all the resistors in both cases have the same resistance, *R*, the currents that pass through the resistors, R1-R12, are the same in both network types, and no current passes through R13-R18 in the branched-network. Since the resistance of NW junctions are likely to be different at the beginning of Joule heating, it is important to learn how the different resistance affects the heating power at NW junctions. In this study, the resistance of R6 is changed to *2R* or *0.5R* while all the other resistors stay constant. The current that passes through each resistor is calculated, measured and displayed by Simulink and the heating power is calculated using Joule's Law afterwards.

To show the difference in heating power of R6 compared to the rest of the resistors, the ratio of heating power of R6 was taken with respect to the average heating power of R1-R5 and R7-R12. These results are recorded in Table 3.1. The details of current and heating power distribution are listed in Appendix C. When R6=*2R*, R6 generates 42% more and 9% less heating power than the average of the others in the chained and branched networks respectively. When R6=*0.5R*, R6 generates 40% less and more than triple the heating power than the average of the others in the chained and branched networks respectively.

Table 3.1 The ratio of heating power of R6 to the average of the rest of R1-R12

Resistance setting	Ratio in chained networks	Ratio in branched networks
R6=*2R*, the rest=*R*	1.42	0.91
R6=*0.5R*, the rest=*R*	0.60	3.45

In these calculations, a higher resistance generates more heat and a lower resistance generates less heat in chained networks. This may mean Joule heating in chain-connected NWs could improve the connection of higher resistance NW junctions over other junctions. Since these NW junctions may improve faster, the difference between their resistance and other junctions could decrease. Similarly, a lower resistance may generate less heat and improves the conductivity more slowly; thus, the difference between the lower resistance junctions and other junctions is likely to decrease as well. However, the opposite trend may occur in branch-connected NWs; a higher resistance may generate less heat and a lower resistance may generate more heat in the resistor. If this condition exists, it will cause the NW junctions with lower resistance to weld faster and achieve lower resistance. The difference between their resistance and other junctions will then increase. Then NW junctions which have started with a lower resistance will probably get welded and ripened first. Further heating may break the junctions and cause failure, while other junctions still need further heating to weld.

In both cases, currents passing though R13-R18 in the branched networks are much smaller than the ones in R1-R12. On average, the heating power in R13-R18 is less than 1% of the heating power in R1-R12 in both calculations. This is an example that shows that in NW networks, only the NW junctions that are connected in the paths of the main current flow are possibly heated and welded, and the NW junctions not connected in these paths will generate very little heat to improve the conductivity. If the conductivity of all NW junctions requires improvement, a second Joule heating process could be applied.

To summarize, Joule heating may be more suitable for ordered networks that are rich in chain-connected NWs than random NW networks for two reasons. First, NW chains are mainly connected in one direction, which can form the path of current flow; thus, most of the NW junctions are welded at the same time. Second, NW chains have many chain-

connected NWs, in which a junction with higher resistance may generate more heat and benefit the welding process. In contrast, random NW networks usually have many branch-connected NWs, in which a junction with low resistance is very likely to generate more heat and be welded before other junctions.

3.3 Experiments

After ordered NW networks were created on polymer substrate using the method described in Chapter 2, the sheet resistance of each channel was measured by Keithley 6430 SUB-FEMTOAMP REMOTE SourceMeter, using 4-point auto mode. Joule heating was conducted to improve the conductivity. The 4-point manual mode of the same device allows us to control the current while measuring the resistance. A current of 50mA with 21V compliance voltage was chosen for Joule heating and the resistance was recorded manually until the resistance no longer decreased or suddenly became extremely high, i.e. the NW chains were broken. The resistance was then converted into sheet resistance.

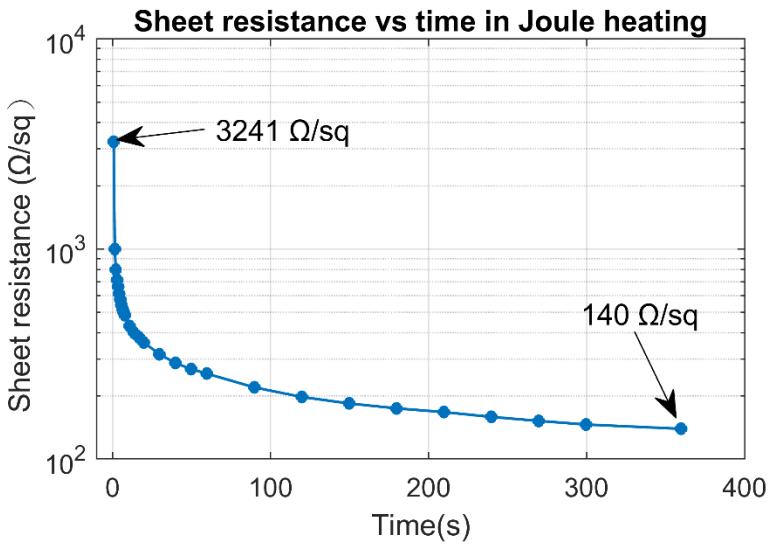

Figure 3.3 Sheet resistance of ordered NW networks changed during Joule heating process

Figure 3.3 shows an example of how the sheet resistance of ordered NW networks changed in the process of Joule heating. The sheet resistance of NW chains decreased significantly during Joule heating process within a few minutes. SEM pictures taken after Joule heating show welded NW-junctions, as shown in Figure 3.4. NW junctions were welded by Joule heating for two reasons. First, the heating locally melts the NWs at the junctions. Second,

the current was forced through the contact at the junction, causing electromigration of the Ag material. Electromigration is the displacement of atoms caused by momentum transfer from the charge carriers [77].

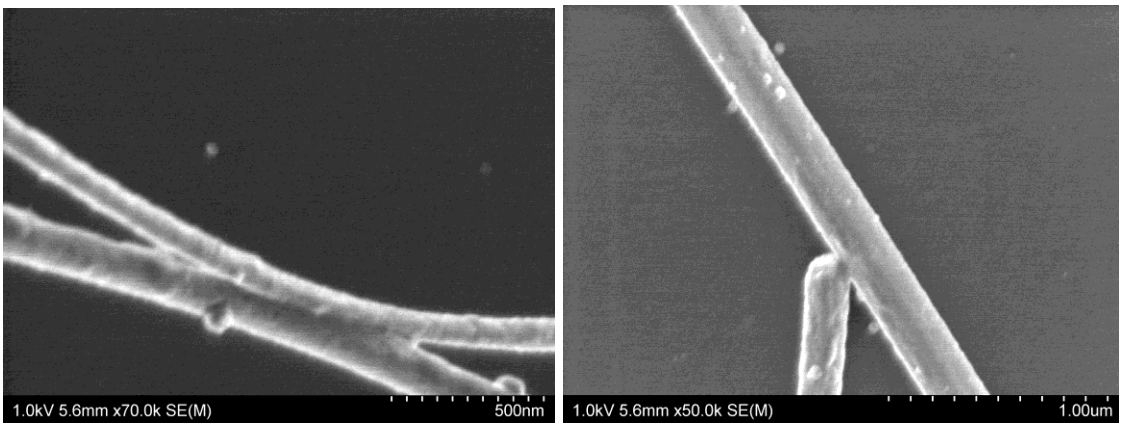

Figure 3.4 Welded NW junctions after Joule heating

3.3.1 Plasma cleaning followed by Joule heating experiments

As it can be observed from the micrographs, ordered NW networks created by the chaining technique also have many branch-connected NWs, possibly due to the curvature of the Ag NWs. As shown in the Simulink calculations, branch-connected NWs create a problem for conductivity improvement of the whole NW networks due to nonuniform Joule heating. One way to reduce the seriousness of this problem is by applying treatment before Joule heating. Another reason to use a treatment before Joule heating is that Joule heating itself can only improve the conductivity of the junctions on the percolative paths, which the current will pass through. The current will not pass through other parts of the networks, and thus can not improve the conductivity of those junctions. These NW sections that are not on the percolative paths can still be important; for example, they can collect free carriers when being used as transparent electrodes in solar cells [78].

Table 3.2 Electrical properties of ordered NW networks before and after Joule heating for different NW concentration, after 20min plasma cleaning.

Concentration (mg/mL)	Transmission (%)	Rs(Ω/□)	
		Before Joule heating	After Joule heating
0.25	95.4	30.6	27.0
0.35	94.0	29.3	23.5
0.45	92.3	38.6	20.3

Plasma cleaning is an effective way to remove PVP without damaging the NW networks or the polymer substrates [79]. In this experiment, ordered NW networks with different concentrations were fabricated on polyimide substrates, and then they are cleaned with plasma for 20min. The light transmittance and sheet resistance were measured and recorded. Then networks in each channel were Joule heated by a DC current of 50mA for 30s. The sheet resistance was measured again and recorded. Table 3.1 shows comparison of sheet resistance before and after Joule heating. Note that 7 samples of NW networks were created for each concentration, and transmittance and sheet resistance shown are mean values.

Considering that ordered NW networks typically have a sheet resistance higher than 10 kΩ/sq after deposition, most of the sheet resistance reduction was achieved by plasma cleaning. Joule heating was able to further reduce the sheet resistance. Among the 21 samples, Joule heating of 50mA for 30s further reduced the sheet resistance by a range of 8-72%, and the mean value is 32%. However, 2 samples of the 0.25mg/mL concentration failed during the 30s Joule heating.

3.3.2 Sweep voltage experiment

At the very beginning of Joule heating, the resistance dropped greatly, as shown in Figure 3.3. Sweep voltage experiments were done to further analyze the reason. After creating NW chains on polymer, voltage sweeps were run through the NW chains from 0 to 20 V at a step of 0.0805 V, and current was recorded. Multiple sweeps were done, and the results are show in Figure 3.5.

In the first sweep, the current remained at 0 as the voltage increased, at 6.762V, it then increased dramatically to the compliance current. This voltage is called “Threshold voltage” or “surge voltage”. This is a typical characteristic of a dielectric layer sandwiched between two metals, breaking down once a certain voltage is reached [80], which in this case would be NWs sandwich a thin layer of PVP.

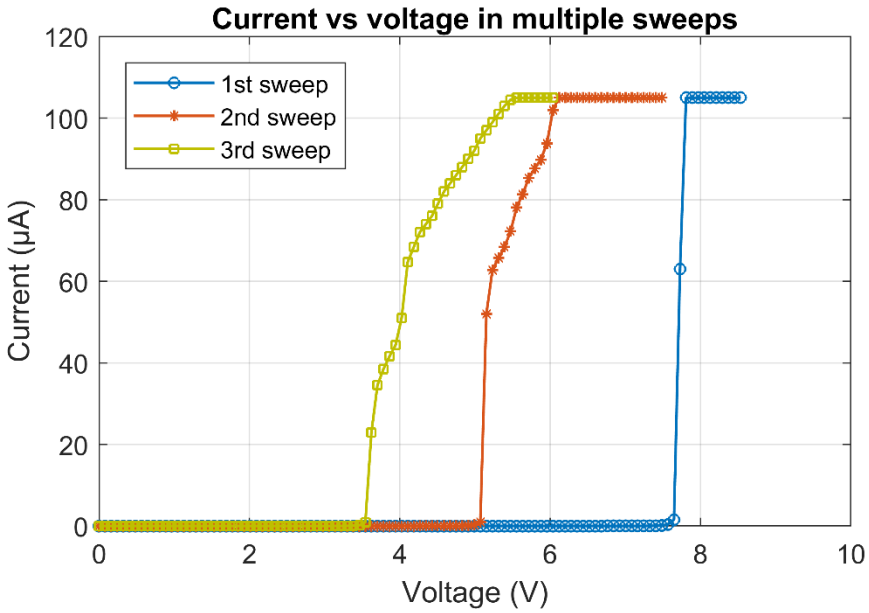

Figure 3.5 Current response during three voltage sweeps

In the second and the third voltage sweeps, I-V curves have similar shapes. However, the threshold voltage drops after every activation. Similar phenomena have been observed in Joule heating experiment with a single Ag NW-junction [80]. The decrease in threshold voltage due to the breakdown of PVP every time current runs through, although very limited current.

During Joule heating process, the compliance voltage was 21 V, which is much higher than the threshold voltage for the first sweep. Therefore, the compliance voltage can break through the PVP layer at the NW junctions and activate the NW chains connection. This explain why the resistance dropped rapidly at the beginning of Joule heating.

After Joule heating, the voltage sweep was conducted, and the result was compared to the first sweep result of NW chains without Joule heating. The sweep characteristic shows that the current starts to increase at the very first step and continues to grow rather steadily.

This is likely caused by PVP breakdown in the current paths in the Joule heating process, so no or very little threshold voltage is needed. Instead, the current-voltage response curve is close to linear, or Ohmic.

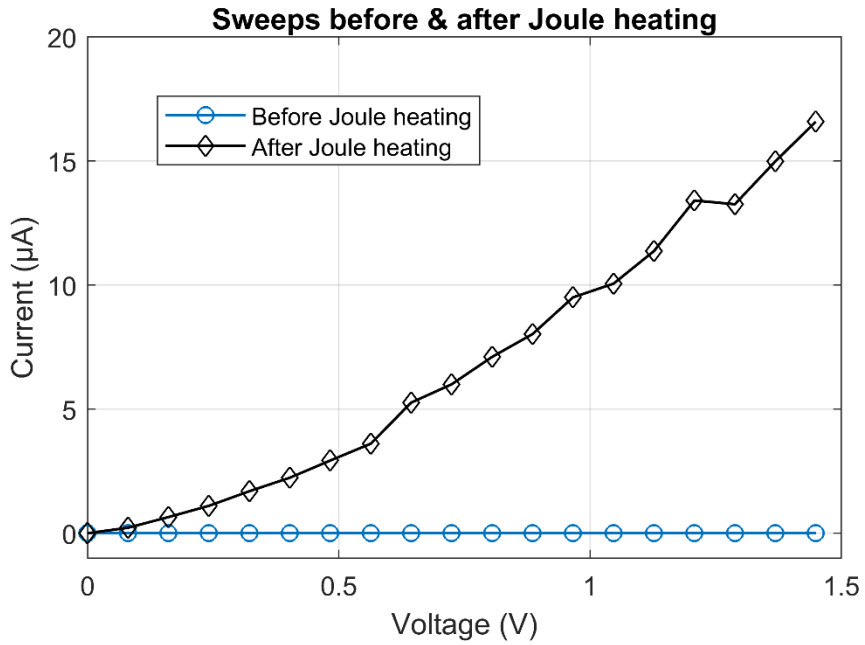

Figure 3.6 Comparison of current-voltage response curves of ordered NW networks before and after Joule heating

3.3.3 NW chains failure after Joule heating

In one study conducted by A. Vafaei et al., it is reported Joule heating is a self-executing process in which the welding mechanism stops automatically at the completion of the weld [81]. This makes sense theoretically because with the decrease of resistance, less over heat will be generated with the same current, and was verified with Joule heating experiment to weld a single junction between two NWs [81]. However, in networks with many branch-connected NWs, it was shown in the simulation that lower resistance junctions generate more heat and thus have the risk of over-heated. It is observed in our experiments that Joule heating for too much time can result in failure of the Ag NWs, just like what was reported with thermal annealing. During Joule heating, the resistance of NW networks suddenly became super high after some time, which is failure of NW networks. The failed NW networks were then observed under SEM for further study, as shown in Figure 3.7.

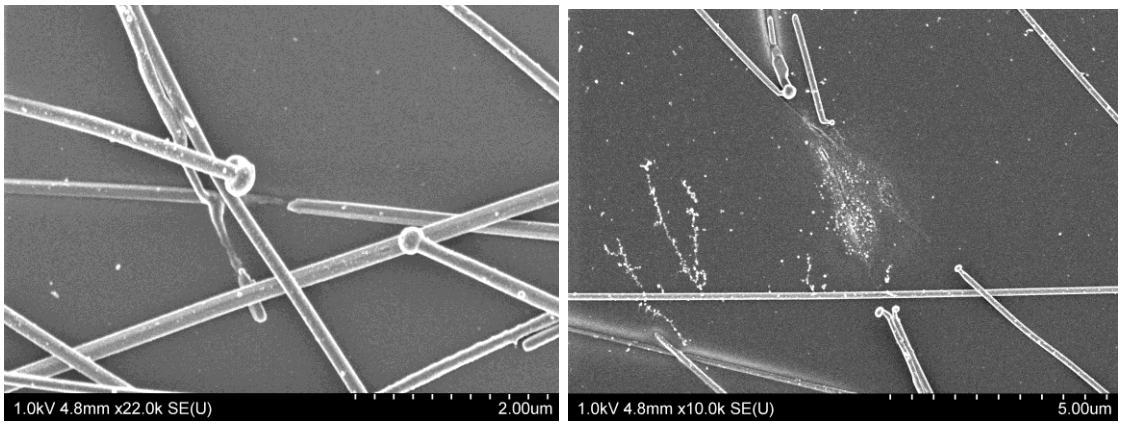

Figure 3.7 SEM pictures of broken NW chains

The broken parts of NW tend to become spheres. This is likely due to the surface tension after melting. When one end of the NW melts, the newly formed sphere stays with the solid part of NW. Small spheres or particles can gather into bigger spheres caused by surface tension.

There are several reasons that could cause the failure of NW networks. First, the accumulation of heat in local areas, especially at the NW-junctions, causes temperature to rise to the melting point of silver at nanoscale. The local melting NWs causes the networks to fail. Second, electromigration could induce void spots at the NW-junctions, resulting in disconnection in the networks. The generated heat also accelerates the process of electromigration because it increases the atom mobility [77]. Third, Rayleigh Instability slowly changes the shape of NWs and finally leads to failure. Rayleigh Instability has been reported in annealing NWs [82] [83]. The changed shapes of NWs were observed under SEM and shown in Figure 3.8. In Rayleigh Instability, the distance between two concave spots is called wavelength [82]. Since junctions have the most heat generated, and the shape of a NW probably changes at the junctions first and notes were then formed. It is possible that when the distance between two junctions is close to an integral number of the wavelength, the NW becomes more vulnerable to Rayleigh Instability.

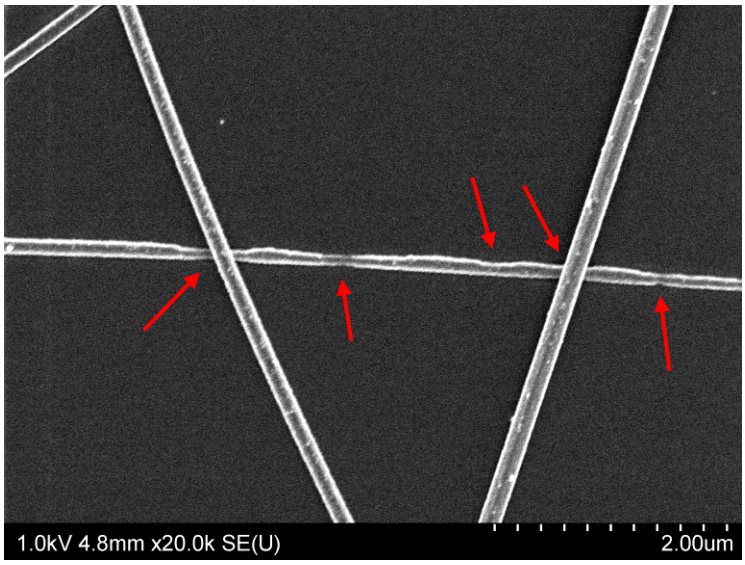

Figure 3.8 SEM picture of shape of NWs after Joule heating. The horizontal NW in this picture has several concave spots, as pointed out by the red arrows.

3.4 Conclusions

Joule heating itself can improve the conductivity of ordered NW network significantly. However, during Joule heating, current distributes unevenly due to the branched connection among NWs. Non-uniform current causes varied heat generation so only a portion of NW junctions are likely to be welded before failure occurs.

Treatments such as plasma cleaning followed by Joule heating are a beneficial way to further improve conductivity. Among the 21 samples in the experiment, Joule heating of 50mA for 30s further reduce the sheet resistance by a range of 8-72%, while 2 samples failed.

Although Joule heating can further improve the conductivity of NW networks, it has a risk of failure. Since plasma cleaning can decrease the sheet resistance from more than 10kΩ/sq to 10s Ω/sq, to avoid sample failures, experiments in the following chapters only use 20min of plasma cleaning as post-treatment.

Chapter 4 NW chaining on PET: simulations & experiments

Although ordered NW networks have been created successfully on polyimide as shown in Chapter 2, it is very hard to handle because it rips and wrinkles easily. A thicker and more rigid polymer can be used to replace polyimide. In this chapter, an alternative polymer is explored; PET thin film is used as flexible substrates for NW chaining.

4.1 Polymer alternative

The polymer used in the experiments is polyimide. The advantages of polyimide are that it bonds to the glass and is very thin. The thickness of polyimide spin coated at 3500rpm is about 7μm. The disadvantage is that once it is peeled off the rigid substrate, it becomes wrinkled and difficult to reattach. This is problematic since the process of peeling and reattaching will be needed for it to be used in a practical application. Polyimide also has a light-yellow color which affects the light transmittance.

A good polymer candidate for NW chaining should be flexible, thin, and transparent. It should also be slightly stiff so that is does not wrinkle easily. One option is polyethylene terephthalate (PET) thin film. In consideration of the material being easy to handle and thin, PET film with a thickness of 23μm were purchased from GoodFellow Inc for experiments.

The change in polymer causes a difference in material and thickness, which will affect the AC electric field applied on the NW suspension for the chaining process. What material properties will affect the field? How would the field change with polymer thickness? These questions need to be answered.

4.2 COMSOL simulations of electric field on PET

Electric field distribution for the NW suspension is very important in controlling the chaining process of NWs. Simulations of the electric field were done with COMSOL Multiphysics software – a Finite Element Analysis (FEA) tool to study how the field distribute, and how it changes with different PET thickness and the gap size of the electrodes.

Since the electric field does not change along the direction of interdigitated electrodes except the area near the ends of the electrodes, acquiring electric field distribution can be simplified as a 2D problem. A 2D case was built in COMSOL Multiphysics 5.2 and the electric current module (under AC/DC Module) is used to investigate the problem. The software uses a mesh builder to divide the solving region into many triangles, and then solves the partial differential equations in the triangular solving regions. The solving region in this simulation consists of a substrate, electrodes, a PET layer, IPA suspension, and an air layer. The boundary condition of the entire solving region is charge conservation. 12 electrodes were horizontally distributed according to the gap size, and harmonious voltages with the amplitude of 10V was applied to each electrode. Due to the large number of electrodes built in the simulation the boundary effect on the simulation results could be ignored. A test of 24 electrodes was simulated and the difference of electric field strength at the center was less than 0.1%. The other possible approach to eliminate the effect of boundary conditions is using periodic boundary conditions. Note that these simulations of PET have not considered any effect from NW dipoles, and the polymer is considered well attached to the electrodes and glass. The frequency, PET thickness and gap size are variables which were studied.

4.2.1 Results and discussion

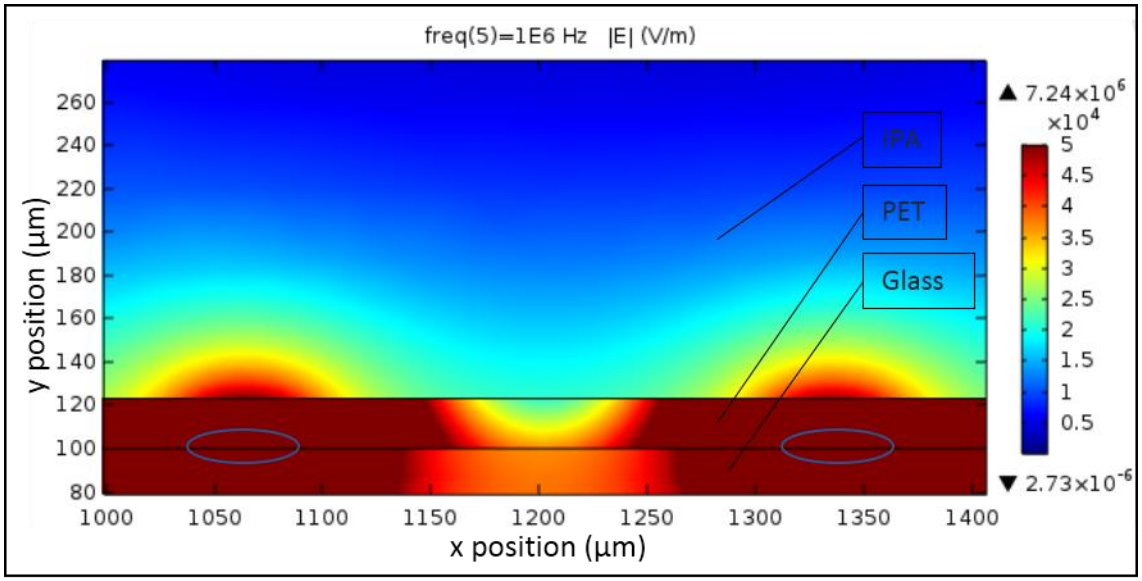

Figure 4.1 A contour map that shows the magnitude of the electric field when the applied frequency is 1MHz, gap size is 240µm, and PET thickness is 23µm. The positions of electrodes were circled.

Figure 4.1 shows a contour plot of the field strength distribution across two electrodes as well as the polymer and alcohol above them. The highest electric field strength is located near the electrodes, as expected, but electric field strength drops dramatically from the PET to alcohol. Field strength also decreases significantly across the alcohol in the height direction, and it reaches 10000V/m at near 90µm above the PET over the electrode region, and at near 50µm over the gap center region.

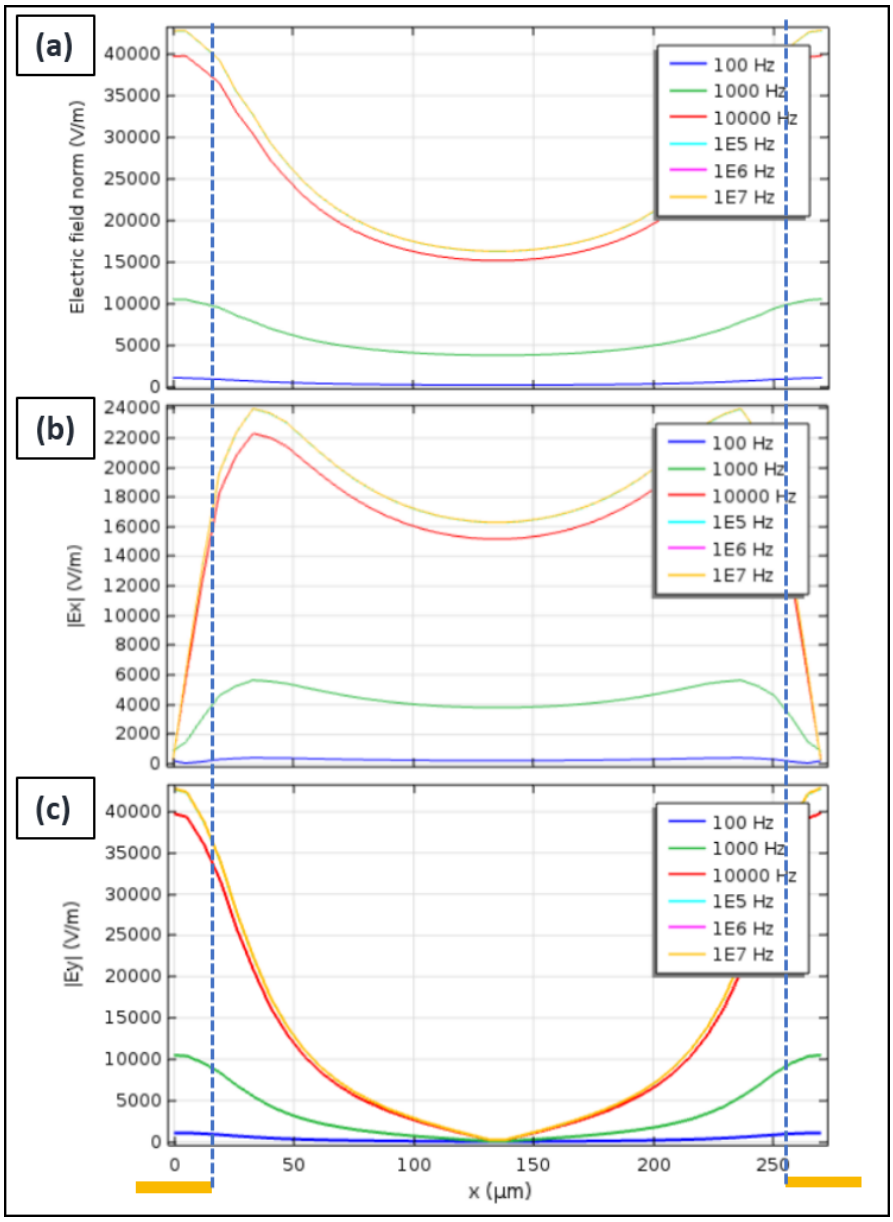

Figure 4.2 The electric field strength and its x and y components at 5µm distance above the PET surface between the centers of two electrodes, for different frequencies. The gap size is 240µm, and PET thickness is 23µm. The position of the electrodes were indicated by the yellow rectangles.

To investigate the effect of different frequencies, simulations were done with frequencies ranging from 100Hz to 10MHz. The field strengths at a 5µm distance above the polymer were recorded as shown in Figure 4.2. The electric field strength is strongest above the electrodes, and weakest at the centre of the gap. The x-component of the field is 0 above

the electrode center and has the highest value at approximately 15μm away from the electrode edges. The y-component of the field is 0 at the centre of the gap and has the highest value above the electrodes. With the increase in frequency from 100Hz to 100kHz, the electric field strength increases. The field strength remains constant at frequencies higher than 100kHz. This is because with the increase in frequency, the impedance of the polymer decreases, which lowers the voltage imposed on the polymer. This allows a higher voltage on the NW suspension, and thus increases the electric field strength. The lowest field strength at a frequency of 100kHz or above is around 15000V/m.

4.2.2 Parametric studies on the field strength at gap centre

Since the lowest field strength occurs at the centre of the gap, this strength has to be high enough so that the dipole-dipole interaction at that region is strong enough to connect NWs into chains. Therefore, it is essential to track how this strength changes with the variables. It is expected that field strength will drop with the increase of polymer thickness. We conducted a parametric study in COMSOL for PET thickness from 5 to 160μm, and the resulting field strengths at the gap center are plotted in Figure 4.3. The detailed distribution of the electric field strength is shown in Figure E.1. Electric field strength at the gap center decreases logarithmically with the thickness of PET. This means every time the PET thickness doubles, the field strength at the gap center will drop by a certain value, approximately 4444V/m in this case.

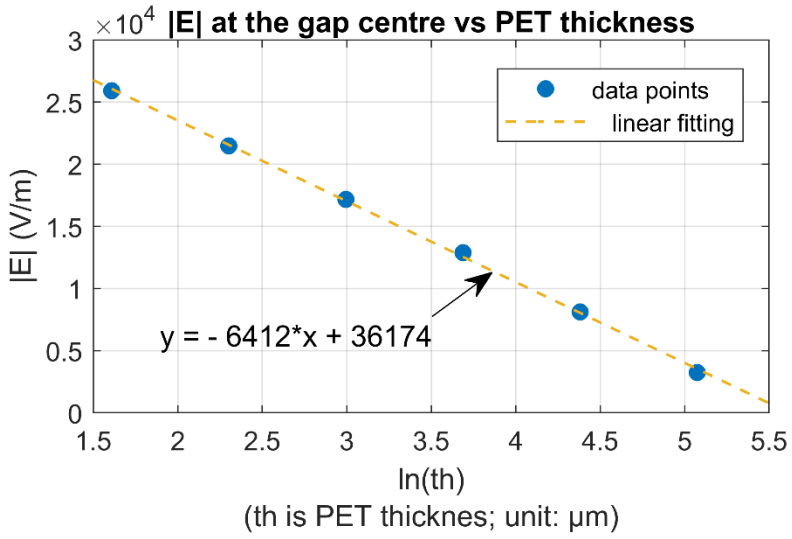

Figure 4.3 Electric field strength at the gap center changes with the thickness of PET. The frequency for simulation is 1MHz, the voltage is 20Vpp, and the gap size is 240μm.

Another parametric study in COMSOL varies the gap sizes between electrodes. There are substrates of 6 different gap sizes ranging from 120μm to 420μm fabricated for the experiments, therefore the simulations also use these 6 gap sizes. The results are plotted in Figure 4.4. With the increase of gap size, the electric field strength is expected to decrease. In the plot, ln(|E|) decreases linearly with ln(gap), which means the field strength at the gap center has a power law relationship with the gap size. We wanted to know if this relationship is consistent with different conditions such as polymer thickness, frequency, polymer existence. The different gap sizes were simulated on 7μm polyimide with 100kHz frequency, and also directly on the substrate with 10kHz were simulated. The results show that there is a power law relationship between field strength at the gap center and the gap size for all three cases, as shown in Figure 4.4. Simulation results of the field strength distribution for these three scenarios are included in Appendix D. The functions are $|E| = 1.09 \times 10^6 \times (gap)^{-0.77}$ for 23μm PET with 1MHz frequency, $|E| = 4.24 \times 10^6 \times (gap)^{-0.94}$ for 7μm polyimide with 100kHz frequency, and $|E| = 1.71 \times 10^7 \times (gap)^{-1.11}$ for no polymer with 10kHz.

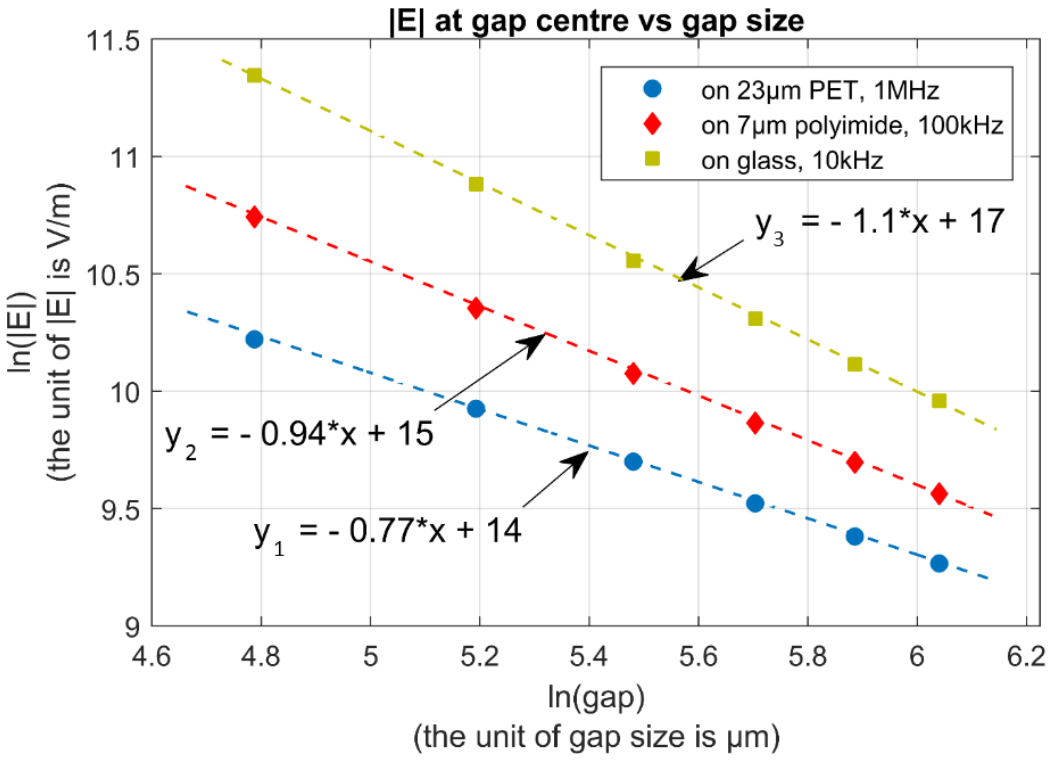

Figure 4.4 ***ln(\|E\|)*** **decreases linearly with** ***ln(gap)*****, within the gap size range of 120 -420µm. The lines are linear fitting results for different conditions.**

In an ideal parallel electrodes model without polymer in a DC circuit, the formula for the electric field strength, *E*, is:

$$E = \frac{V}{d}, \tag{23}$$

where *V* is the voltage and *d* is the distance between the parallel electrodes. *E* has an inverse proportional relationship with *d*. When the *d* doubles, the electrical field strength halves. Inverse proportional function is actually a special type of power function, with the exponent equaling to -1. So, if *ln(E)* is plotted with respect to *ln(d)*, it would result in a linear line with -1 slope. The *d* in parallel electrodes case shares similar physical meaning to the gap size in this study. In the fitting functions for 23µm PET and 7µm polyimide, the exponents are -0.77 and -0.94, respectively. These values are larger than -1, which means when the gap size doubles, the electrical field strength is higher than half of the original

value. But in the formula for glass, the slope is -1.11, which is smaller than -1, meaning when the gap size doubles, the electrical field strength is lower than half of the original value.

4.3 Experiments of NW chaining on PET

PET itself is not adhesive. There are two ways to attach a PET thin film to a glass substrate. One is by attaching the PET film with a static cling layer, which adheres the film to the glass substrate by electrostatic forces. This method is used in screen protectors and window design covers. The other way is by attaching the PET film to the glass substrate by capillary forces using a drop of liquid, such as water or oil. The second method is easier to realize. Since oil is messier and may need a follow up cleaning step, water was chosen for the experiments.

The experiment setup for NW chaining is the same as in Chapter 2, but instead of spin coating the polymer on the substrate with interdigitated electrodes, PET is attached on the substrate by a drop of water. Ordered NW networks were created with the size of 1mm×10mm within dam channels. After the NW chaining process, the PET sheet with ordered NW networks is peeled off from the substrate.

Firstly, a harmonic voltage with 7Vrms and 100kHz frequency was applied. The experiments have seen severe disruption from fluid motion near the sides of the channel walls. This resulted in very few NW chains in the middle region of the channels on the PET after alcohol drying. The average sheet resistance was measured to be about 500 Ω/sq. The fluid motion is suspected to be caused by the electroosmotic effect [13]. The electroosmotic effect can be reduced by increasing the frequency. However, the frequency available in our laboratory is limited by the Tektronix CFG253 function generator. As shown in Figure 4.5, after the frequency reaches 1MHz, the maximum voltage decreases rapidly with the increase of frequency. Therefore, the 1MHz frequency, and the corresponding highest voltage, 6.5Vrms, was applied for NW chaining on PET. There was still circular motion near the channel walls, but much less violent. Figure 4.6 shows the arrangement of NWs under SEM. The NW suspension concentration is 0.25mg/mL, and the gap size of interdigitated electrodes is 360μm.

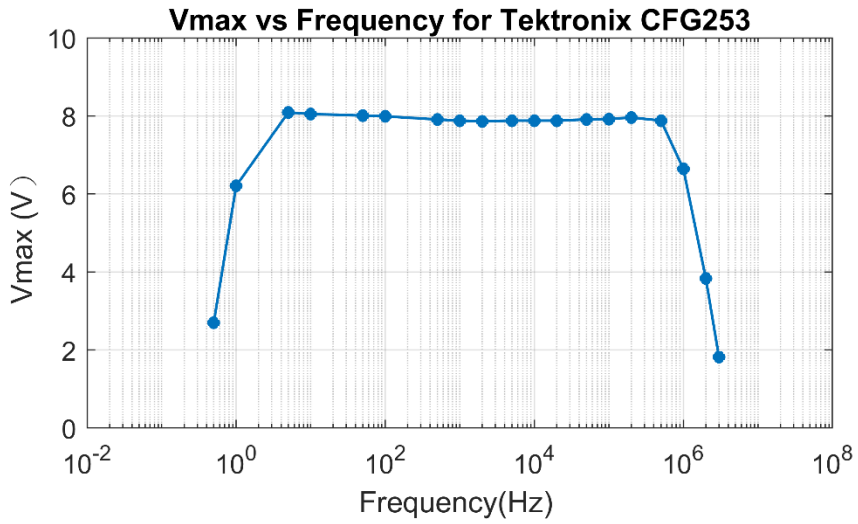

Figure 4.5 The highest RMS voltage available at different frequency for Tektronix CFG253 function generator

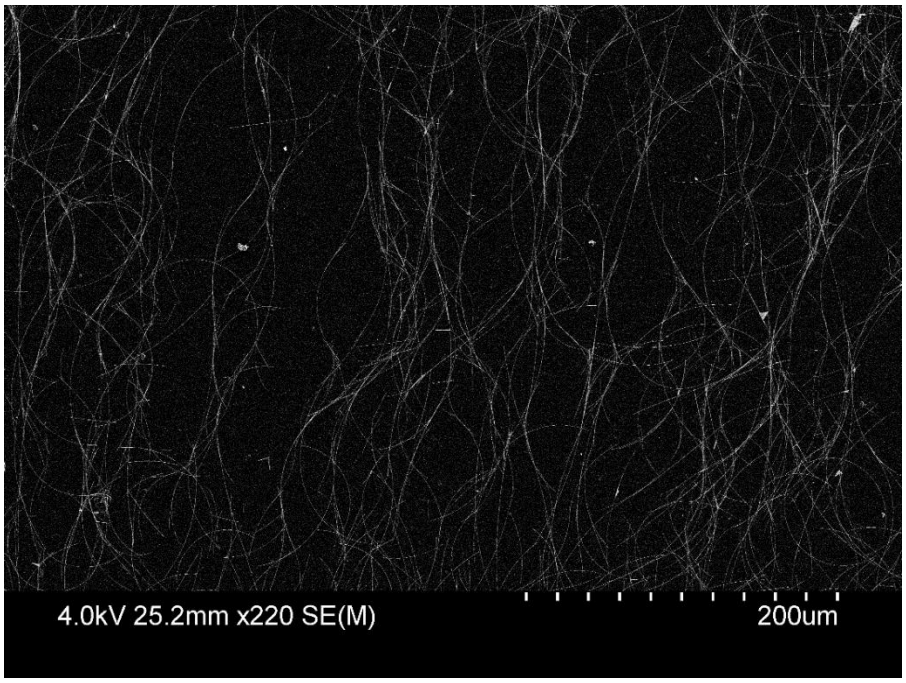

Figure 4.6 A SEM picture of ordered NW networks deposited on PET.

The fluid motion near the channel wall is visible under an optical microscope, and a video was recorded. As introduced in Chapter 2, the electroosmotic flow is one of the disrupters during the NW chaining process. However, the fluid flow seen was in a different direction from the electroosmotic movement as shown in Figure 4.7. The electroosmotic movement

circulates in the plane that is perpendicular to the interdigitated electrodes, while the fluid flow seen in the experiment circulates in the plane that is parallel to the interdigitated electrodes. It is possible that the electroosmotic movement interacts with the channel wall, which changes its circulating direction. Figure 4.8 shows the NW networks near a channel wall. There are fewer NW chains formed between the gap near the channel wall, due to the disturbance of the fluid motion during the NW chaining process.

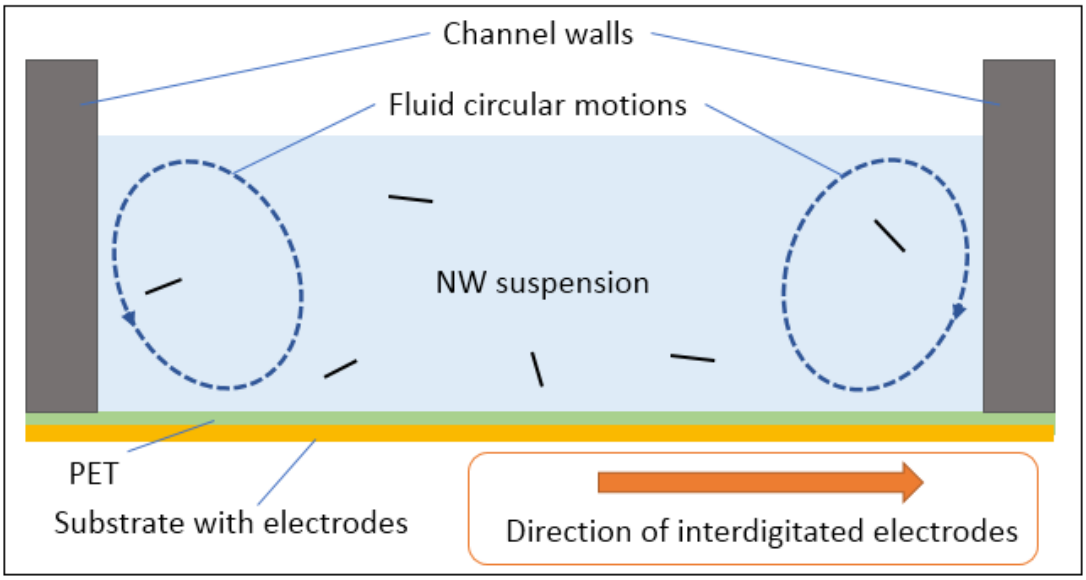

Figure 4.7 Illustration of the fluid circular motions near the channel walls

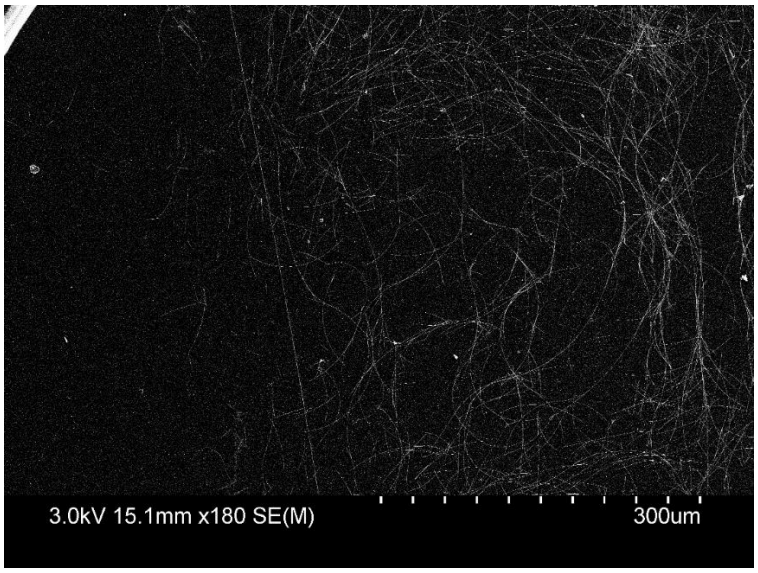

Figure 4.8 A SEM picture of NW networks near the channel wall. NWs orientation is less ordered at this region, and less NW chains have been built across the gap. The gap size for this sample is 360μm.

4.3.1 Parametric experiments with different gap sizes

If the polymer thickness, applied voltage, and frequency are chosen, the most important parameter that affects the electric field is the gap size between interdigitated electrodes. To explore what is the most suitable gap size for NW chaining on PET, an experiment of NW chaining with gap size from 120 – 420μm was done. The sheet resistance of the resulting ordered NW networks was measured and compared, as shown in Figure 4.9. The NW concentration for all samples used was 0.25mg/mL.

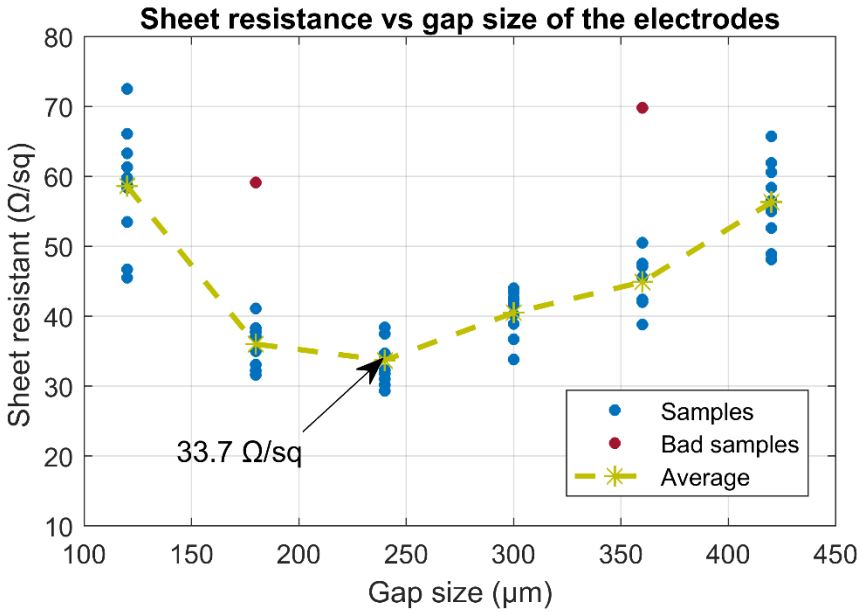

Figure 4.9 Sheet resistance of ordered NW networks created using different gap size. The dots represent results of experiment samples, and the two red dots represent two samples that have big NW clumps, and they were excluded when calculating the average sheet resistance.

With the increase of gap size from 120 to 420μm, the average R_s first decreases and then increases, ranging from 33.7 to 58.6 Ω/sq. At 240μm gap size, the average R_s reaches the lowest value, 33.7 Ω/sq. The corresponding average transparency is 94.2%, for which the reference is the PET sheet. SEM pictures of ordered NW networks created on all 6 different gap sizes were taken to further explain the behavior of the R_s changing, as shown in Figure 4.10. With the increase of gap size, the electric field strength between interdigitated electrodes get weakened, and thus fewer NW chains formed through the gap. This explains why R_s increases when gap size increases from 240 to 420μm. In the range of 120 to 240μm, although a smaller gap size will result in a higher electric field and more NW chains forming, the NW chains between gaps are shorter. The connection of NW chains from one gap to the next is not as effective as the NW chains between electrodes. Therefore, shorter NW chains would not make full use of the advantage of the NW chaining technique, and thus have a higher R_s.

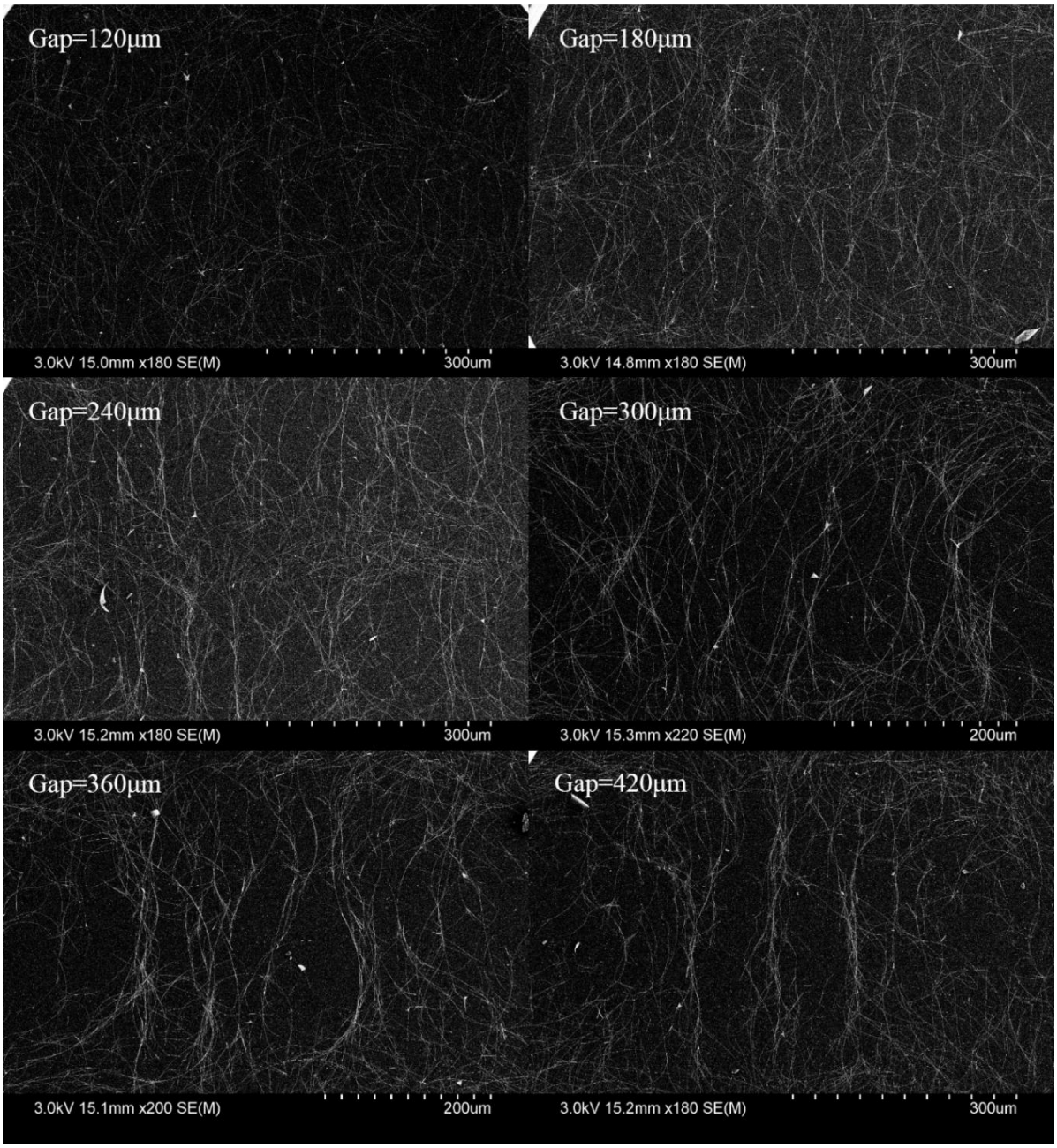

Figure 4.10 Ordered NW networks created using 6 different gap sizes on PET. The larger the gap size, the fewer and longer NW chains formed.

4.4 Conclusions and future work

This chapter explores the effects of thicker polymer and different gap sizes of electrodes through both numerical simulations and experiments. Simulations provide the extent to

which an increase of polymer thickness resulting in a lower electric field strength. The lowest electric field strength occurs at the centre of the gap, and its value decreases logarithmically with the thickness of the polymer. A thicker polymer also requires a high frequency for the NWs to be chained in the experiments. Ordered NW networks were created on 23μm PET. However, due to a weaker field strength applied to the NW suspension on 23μm PET compared to 7μm polyimide, the ordered NW networks on PET show a higher sheet resistance of 36.0Ω/sq. In comparison, the ordered NW networks on polyimide have a sheet resistance of 30.6Ω/sq, with the same NW concentration and gap size.

COMSOL simulations show that the electric field strength at the gap center has a power law relationship with the gap size of the electrodes, both on polymers and on glass substrates. Due to two factors, a smaller gap size enables higher field strength, while a larger gap size allows a higher ratio of effective chaining areas, the sheet resistance of ordered NW networks first increases the gap size and then decreases. With a 240μm gap size, the average sheet resistance reaches the lowest value of 33.7Ω/sq with 94.2% transparency at 550nm. Their FOM is $0.016\Omega^{-1}$, which is lower than the FOM achieved on polyimide, but it is still higher than the FOM of commercial ITO, which is $0.005\Omega^{-1}$

Since the fluid motion weakened when the applied frequency increased from 100kHz to 1MHz, it is affected by the frequency, and likely suppressed by high frequency. If the electronics permit, experiments with higher frequencies than 1MHz should be conducted to test if the fluid motion can be eliminated. Also, the mechanism of the fluid motion requires more research.

Chapter 5 NW chaining in sandwiched channels

Although the NW chaining technique creates obvious NW chains within the dam channels, the free surface of NW suspension allows fluid to move, which affects the quality of the resultant ordered NW networks. In this chapter, we anticipate what would happen to the ordered NW networks if the channels have lids.

5.1Theory

5.1.1 Drawbacks of a regular top-open channel

There are several ways that fluid movement can affect the process of NW chaining. Firstly, due to the surface tension of the fluid, the thickness of NW suspension inside the channels is not uniform; near the channel walls the NW suspension is thicker. This could result in more NWs settling down near the channel walls.

According to the no-slip condition in Fluid Dynamics, when a fluid is in contact with a solid object there will be no relative movement between the layer of fluid at the boundary and the solid surface in contact. Therefore, if the solid surface is stationary, the near-surface fluid has zero velocity. In the NW chaining experiments described in the previous chapters, channels are formed by the dam and the substrate surface. Thus, the NW suspension in contact with the substrate or polymer surface has zero velocity, but the top surface of the NW suspension is free to move, which could cause some disturbance to the NW chaining process.

NW chains that are disturbed and broken are likely to be dragged by DEP forces to the region near the interdigitated electrodes. Therefore, disturbances can increase the percentage of NWs in regions near or on the electrodes. Disturbances also make it hard to form NW chains with large gap to NW length ratio.

5.1.2 Sandwiched channels

In sandwiched channels the top surface of the NW suspension is in contact with another solid stationary surface. Considering the NW suspension is thin, and its movement is limited by two solid surfaces, fluid movement will be much less.

5.2 Experiment setup with sandwiched channels

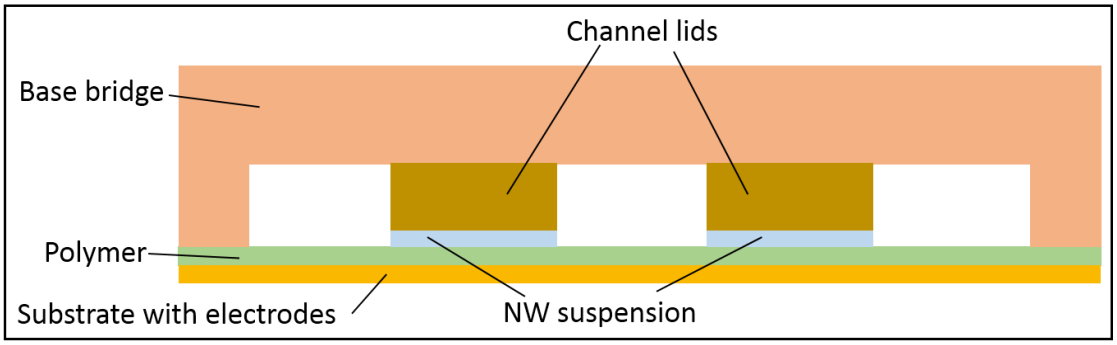

Figure 5.1 Schematic of sandwiched channels in NW chaining process

Channel lids are built on a base bridge. They were design in SolidWorks, and 3D printed using Polylactic acid (PLA). The designed channel height is 0.13mm, and the designed area per channel is 37mm^2. Channel height was measured with a micrometer and calculated to be 0.206mm. The relatively high error of channel height is due to the limited resolution of the 3D printer. Based on the measurement and calculations, 7.5µL of NW suspension was tested to be just the right amount to fill one sandwiched channel.

Experiments of NW chaining were carried out on polyimide and PET. The voltage and frequency for NW chaining on polyimide are 7V and 100kHz, respectively. The voltage and frequency for NW chaining on polyimide are 6.5V and 1MHz, respectively. 7.5µL of NW suspension was injected into each sandwiched channel.

5.3 Results and discussion

With sandwiched channels, multiple Rh NW chains were created over 420µm gap on 7µm polyimide, as shown in Figure 5.2. The Rh NWs were fabricated in our laboratory by a previous PhD student, Nima Moghimian [84]. He measured the NW lengths and calculated the average length to be about 6µm. The ratio of gap size to average NW length is about 70 in this experiment.

NW chains with shorter Rh NWs have been created with open channels, but between gap sizes of no longer than 240µm [85], when the voltage and frequency for NW chaining on polyimide are 7V and 100kHz. NW chaining experiments with open channels between gap

sizes of 360μm and 420μm were conducted, and results were shown in Figure F.4. With the open channels and large gap sizes, some NWs were connected by the field, but no NW chains were formed over the gap size. To summarize, with sandwiched channels, NW chains can be created over larger gap sizes than with open channels. This is due to less fluid disturbance when using sandwiched channels; the required field strength for NW chaining is lower.

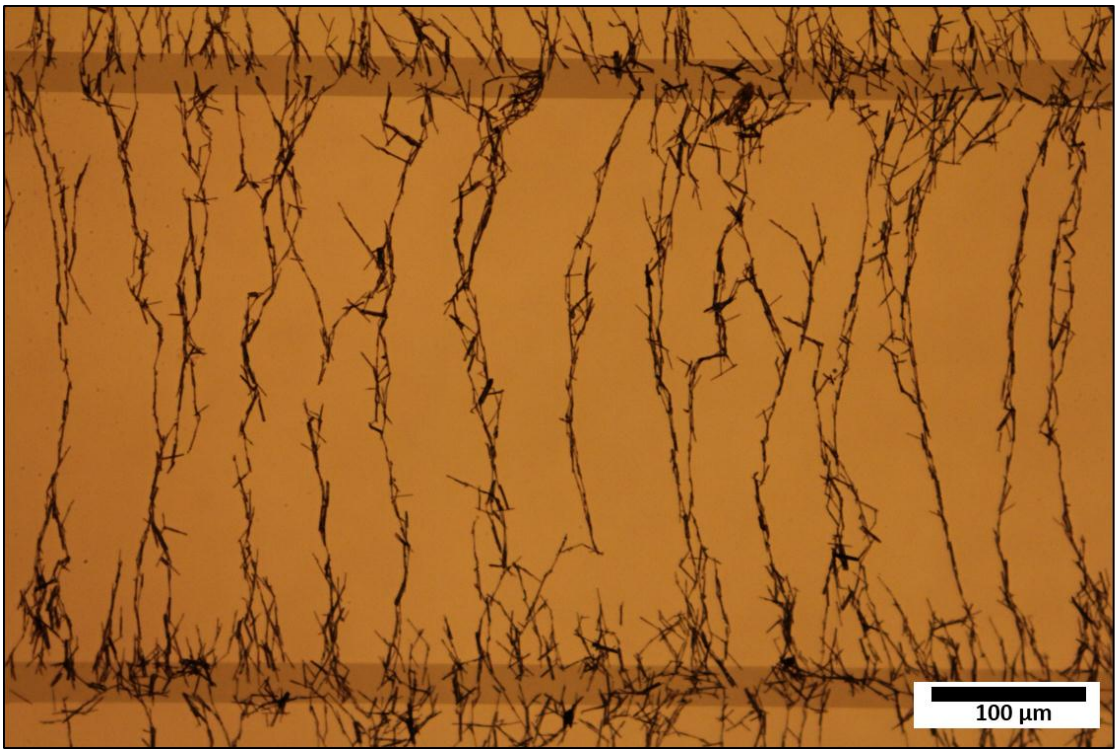

Figure 5.2 A micrograph of ordered Rh NW networks on polyimide fabricated with sandwiched channels. The average length of Rh NWs is 6μm [84]**. The gap size is 420μm. The applied voltage and frequency were 7V and 100kHz, respectively.**

It can be observed from Figure 5.2 that NW chains are almost parallel to each other with some distance, and almost none of the NWs are settled in the space between two NW chains and not connected to at least one of them. In order to study the distance between NW chains, an optical picture that shows a larger area of NW networks was taken. The gap size is 420μm and three gaps of NW chains are studies. There are 26, 30, and 28 NW chains between the top, middle, and bottom gap. The average distance between two NW chains is about 75μm, and the biggest distance between two NW chains is 218μm. Note there are

many branches in the NW chains. In this study, if a branch is longer than half the gap size, it was counted as one NW chain.

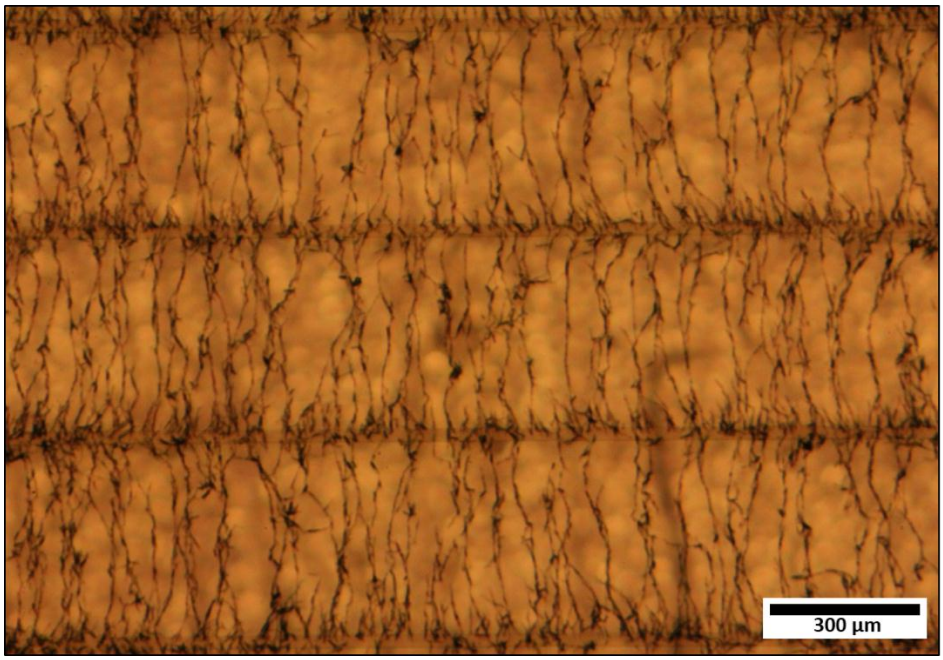

Figure 5.3 Optical picture shows large area of ordered Rh NW networks on polyimide fabricated with sandwiched channels. The actual length and width of NW networks shown are about 2.0 and 1.4mm, respectively.

To evaluate the utilization of NWs in the networks, functional NW chain is defined as NW chains that formed over the gap between electrodes. The length of functional chains and other chain segments was measured in a 1.4mm×0.9mm area. The ratio of functional NW chain length to the total length is 89%. This indicates that about 89% of the NWs were utilized into forming conductive paths in the networks.

Sandwiched channels were also tested successfully in fabricated ordered Ag NW networks on polyimide and PET, and configuration of the resultant networks are shown in Figure F.2 and Figure F.3. Even distribution of NW chains was achieved over both polymer substrates.

5.3.1 Limitations and future work

Due to less area in contact with air, alcohol evaporation is much slower with a sandwiched channel than a regular top-open channel. Generally, it takes 15min for the alcohol to dry

out when using a regular top-open channel, and increasing the NW network area would not affect the drying time. However, when using a regular top-open channel, it takes about 1 hour for alcohol to dry out for a 30mm^2 NW network area. In addition, drying time will scale up with the NW network area.

In future work, channel lips can be a mesh instead of solid surface so that alcohol can be in contact with air and thus shorten the drying time. Another improvement can be made is using tools with higher accuracy than a 3D printer to machine the channel lids and base bridge.

5.4 Conclusions

This chapter introduces the sandwiched channel method in order to reduce the movement of fluid and improve the quality of NW networks. By limiting the fluid movement, NWs are more likely to stay connected to the chains and resist being dragged towards the electrodes by DEP forces, which result in more chains over the electrode gap and more evenly distributed NW networks. The ratio of functional NWs in the ordered networks is therefore increased. In addition, with weak disrupters, NW chains can be created over larger gap sizes with short NWs with the same voltage source.

Chapter 6 Conclusions and future work

This thesis builds on the research that enabled NW chaining established in our laboratory, bringing it into use for creation of TEs, with potential to serve a number of applications. The research includes improvements of the chaining technique and evaluation of the performance of the resultant TEs, through experiments, simulations and modeling. The main conclusions of this thesis are as follows.

1. Ordered NW networks on PET thin films were successfully fabricated with a sheet resistance of 33.7 Ω/sq and 94.2% transparency at 550nm; their FOM is $0.016\Omega^{-1}$, higher than the FOM of commercial ITO, $0.005\Omega^{-1}$. Experiments show that with the increase of the gap size of the interdigitated electrodes, conductance first increases and then decreases, with the highest conductance at the gap size of 240μm. COMSOL simulations show that a thicker polymer decreases the electric field strength, and the electric field strength increases with frequency until a limit value. The electric field strength is at its lowest at the gap centre, and decreases logarithmically with the polymer thickness, while having a power law relationship with the gap size of electrodes.

2. Sandwiched channels were designed and used in experiments for NW chaining to reduce the disruption due to fluid movement. The NW chains look significantly more ordered as a result of chaining in sandwiched channels. About 89% of the NWs were utilized successfully into forming continuous chains over the electrode gaps. In addition, with reduction of the disruptive effect of fluid movement, NW chains can be created over larger gap size with shorter NWs, for the same applied voltage. NW chains were created at a gap to NW length ratio of about 70, which is much higher than the best reported ratio of 40.

3. In the research of Joule heating to improve electrical conductivity of NW chains, the difference of Joule heating with different NW network configuration is

identified. When NWs are connected in chains, higher resistance NW-junctions are likely to generate more heat. In contrast, when NWs are branch-connected, the lower resistance NW-junctions carry higher current and generate more heat, which could result in them being welded before other junctions. Further heating could cause failure of NW networks. Ordered NW networks researched in this work also have many branch-connected NWs; thus, Joule heating itself cannot improve the NW networks to an optimal conductance. 20min plasma cleaning followed by Joule heating with a current density of 50mA for 30sec is tested to be effective in reducing resistance of ordered NW networks while lowering the risk of failures. The improvement by Joule heating varies, and the best improvement seen in experiments is 72%.

4. A mathematical model showed the linear relationship between the transmittance and inverse sheet resistance of perfectly aligned NW chains, and this relationship also sets the upper bound of the performance of NW networks as TEs.

5. We found in experiments that it is difficult to form NW chains positioned directly over the interdigitated electrodes, and this phenomenon can be explained by field distribution results from simulations. Above the electrodes, the gradient of field and the horizontal component of the field, both decrease to near zero, which leads to low value of the director force required for NW chaining. In addition, the NW ends in this region have the same polarity due to the symmetric electric field, and thus they tend to repel each other when they reach the region above the electrode centre. A possible approach for this problem is chaining NWs in two steps, in which the second step is used to bridge the gap with NWs.

In addition to the suggestions for future work that has been included at the end of Chapter 4 and 5, this work could be extended in the following directions.

1. Parameterizing the variation of NW dimensions and shape. In the mathematical models, NWs were assumed to be straight cylinders with the same diameter and length. However, it is difficult to fabricate uniform and identical NWs. NWs used in experiments in this work or other literature vary in diameter, length and amount of curvature. Therefore, it is meaningful to study how the distribution of shape and size could affect the model and results.
2. Haze measurement. Haze measures the percentage of forward-scattered light, (beyond $\pm 2.5^{o}$ from the normal) through a TE. Haze is beneficial in the application to solar cells because scattered light increases the length that light travels in the active layer. Haze lowers the quality of displays when the TE is used in touch screens, thus haze is required to be below 1%. Different applications have different requirements for haze. Therefore, it is important to study how to tune haze so that NW networks can be used for different applications.
3. Experiments tuned for the different needs of applications such as solar cells and touch screens, should be undertaken to maximize the usefulness of NW chain based transparent electrodes.
4. Investigation of the effect of gaps between NWs or broken chains. The effects of gaps or broken chains need to be better understood. They may be associated with charge storage, discharge and dissipative effects that could be modeled by impedances, with resistive and capacitive components. Such models may help us understand how currents distribute over the NW networks.

Bibliography

[1] E. Verploegen, R. Mondal, C. J. Bettinger, S. Sok, M. F. Toney, and Z. Bao, "Effects of thermal annealing upon the morphology of polymer-fullerene blends," *Adv. Funct. Mater.*, vol. 20, no. 20, pp. 3519–3529, 2010.

[2] M. R. Bhalla and A. V. Bhalla, "Comparative Study of Various Touchscreen Technologies," *Int. J. Comput. Appl.*, vol. 6, no. 8, pp. 12–18, 2010.

[3] J. A. Castellano, "The story of liquid crystal displays and the creation of an industry. Hackensack." NJ: World Scientific, 2005.

[4] R. Baetens, B. P. Jelle, and A. Gustavsen, "Properties, requirements and possibilities of smart windows for dynamic daylight and solar energy control in buildings: A state-of-the-art review," *Sol. Energy Mater. Sol. Cells*, vol. 94, no. 2, pp. 87–105, 2010.

[5] J. Kang *et al.*, "High-performance graphene-based transparent flexible heaters," *Nano Lett.*, vol. 11, no. 12, pp. 5154–5158, 2011.

[6] H. Qin, Y. Cai, J. Dong, and Y.-S. Lee, "Direct Printing of Capacitive Touch Sensors on Flexible Substrates by Additive E-Jet Printing With Silver Nanoinks," *J. Manuf. Sci. Eng.*, vol. 139, no. 3, p. 031011, 2016.

[7] R. Newman, "Visible light from a silicon p− n junction," *Phys. Rev.*, vol. 100, no. 2, p. 700, 1955.

[8] H. Kim *et al.*, "Electrical, optical, and structural properties of indium–tin–oxide thin films for organic light-emitting devices," *J. Appl. Phys.*, vol. 86, no. 11, pp. 6451–6461, 1999.

[9] A. Kumar and C. Zhou, "The race to replace tin-doped indium oxide: which material

will win?," *ACS Nano*, vol. 4, no. 1, pp. 11–14, 2010.

[10] U.S. Geological Survey (USGS), "Indium Statistics and Information," 2018. [Online]. Available: https://minerals.usgs.gov/minerals/pubs/commodity/indium/. [Accessed: 09-Oct-2018].

[11] M. Sam, "Controlling field-directed assembly of nanowires: towards nanomanufacturing for biosensors and transparent electrodes," University of Victoria, 2016.

[12] J. Alsaif, "Parametric studies of field-directed nanowire chaining for transparent electrodes." 2017.

[13] M. Sam, N. Moghimian, and R. B. Bhiladvala, "Field-directed chaining of nanowires: Towards transparent electrodes," *Mater. Lett.*, vol. 163, pp. 205–208, 2016.

[14] H. Hosono and D. C. Paine, *Handbook of transparent conductors*. Springer Science & Business Media, 2010.

[15] K. Ellmer, "Past achievements and future challenges in the development of optically transparent electrodes," *Nat. Photonics*, vol. 6, no. 12, p. 809, 2012.

[16] T. Minami, "Transparent conducting oxide semiconductors for transparent electrodes," *Semicond. Sci. Technol.*, vol. 20, no. 4, p. S35, 2005.

[17] D. Zhang, Z. Deng, J. Zhang, and L. Chen, "Microstructure and electrical properties of antimony-doped tin oxide thin film deposited by sol–gel process," *Mater. Chem. Phys.*, vol. 98, no. 2–3, pp. 353–357, 2006.

[18] J. Du, S. Pei, L. Ma, and H. Cheng, "25th anniversary article: carbon nanotube-and graphene-based transparent conductive films for optoelectronic devices," *Adv.*

Mater., vol. 26, no. 13, pp. 1958–1991, 2014.

[19] D. S. Hecht, L. Hu, and G. Irvin, "Emerging transparent electrodes based on thin films of carbon nanotubes, graphene, and metallic nanostructures," *Adv. Mater.*, vol. 23, no. 13, pp. 1482–1513, 2011.

[20] D. Li, W. Windl, and N. P. Padture, "Toward site-specific stamping of graphene," *Adv. Mater.*, vol. 21, no. 12, pp. 1243–1246, 2009.

[21] K. S. Kim *et al.*, "Large-scale pattern growth of graphene films for stretchable transparent electrodes," *Nature*, vol. 457, no. 7230, pp. 706–710, Feb. 2009.

[22] J. Wu *et al.*, "Organic light-emitting diodes on solution-processed graphene transparent electrodes," *ACS Nano*, vol. 4, no. 1, pp. 43–48, 2009.

[23] L. F. C. Pereira, C. G. Rocha, A. Latgé, J. N. Coleman, and M. S. Ferreira, "Upper bound for the conductivity of nanotube networks," *Appl. Phys. Lett.*, vol. 95, no. 12, p. 123106, 2009.

[24] D. S. Hecht *et al.*, "High conductivity transparent carbon nanotube films deposited from superacid," *Nanotechnology*, vol. 22, no. 7, p. 75201, 2011.

[25] Y. Li, "Conducting polymers," in *Organic Optoelectronic Materials*, Springer, 2015, pp. 23–50.

[26] Y. Xia, K. Sun, and J. Ouyang, "Solution-processed metallic conducting polymer films as transparent electrode of optoelectronic devices," *Adv. Mater.*, vol. 24, no. 18, pp. 2436–2440, 2012.

[27] X. Zhang, J. Wu, J. Wang, J. Zhang, Q. Yang, and others, "Highly conductive PEDOT: PSS transparent electrode prepared by a post-spin-rinsing method for efficient ITO-free polymer solar cells," *Sol. Energy Mater. Sol. Cells*, vol. 144, pp.

143–149, 2016.

[28] J. Zou, H.-L. Yip, S. K. Hau, and A. K.-Y. Jen, “Metal grid/conducting polymer hybrid transparent electrode for inverted polymer solar cells,” *Appl. Phys. Lett.*, vol. 96, no. 20, p. 96, 2010.

[29] C. Mayousse, C. Celle, A. Carella, and J.-P. Simonato, “Synthesis and purification of long copper nanowires. Application to high performance flexible transparent electrodes with and without PEDOT: PSS,” *Nano Res.*, vol. 7, no. 3, pp. 315–324, 2014.

[30] W. Hong, Y. Xu, G. Lu, C. Li, and G. Shi, “Transparent graphene/PEDOT–PSS composite films as counter electrodes of dye-sensitized solar cells,” *Electrochem. commun.*, vol. 10, no. 10, pp. 1555–1558, 2008.

[31] D. S. Ghosh, L. Martinez, S. Giurgola, P. Vergani, and V. Pruneri, “Widely transparent electrodes based on ultrathin metals,” *Opt. Lett.*, vol. 34, no. 3, pp. 325–327, 2009.

[32] M. Kang, M. Kim, J. Kim, and L. J. Guo, “Organic solar cells using nanoimprinted transparent metal electrodes,” *Adv. Mater.*, vol. 20, no. 23, pp. 4408–4413, 2008.

[33] F. M. Wisser, K. Eckhardt, W. Nickel, W. Böhlmann, S. Kaskel, and J. Grothe, “Highly transparent metal electrodes via direct printing processes,” *Mater. Res. Bull.*, vol. 98, pp. 231–234, 2018.

[34] J. Van De Groep, P. Spinelli, and A. Polman, “Transparent conducting silver nanowire networks,” *Nano Lett.*, vol. 12, no. 6, pp. 3138–3144, 2012.

[35] J. Hu, T. W. Odom, and C. M. Lieber, “Chemistry and physics in one dimension: synthesis and properties of nanowires and nanotubes,” *Acc. Chem. Res.*, vol. 32, no.

5, pp. 435–445, 1999.

[36] S. De *et al.*, "Silver Nanowire Networks as Flexible, Transparent, Conducting Films: Extremely High DC to Optical Conductivity Ratios," *ACS Nano*, vol. 3, no. 7, pp. 1767–1774, 2009.

[37] S. B. Sepulveda-Mora and S. G. Cloutier, "Figures of merit for high-performance transparent electrodes using dip-coated silver nanowire networks," *J. Nanomater.*, vol. 2012, p. 9, 2012.

[38] L. Hu, H. S. Kim, J.-Y. Lee, P. Peumans, and Y. Cui, "Scalable coating and properties of transparent, flexible, silver nanowire electrodes," *ACS Nano*, vol. 4, no. 5, pp. 2955–2963, 2010.

[39] V. Scardaci, R. Coull, P. E. Lyons, D. Rickard, and J. N. Coleman, "Spray deposition of highly transparent, low-resistance networks of silver nanowires over large areas," *Small*, vol. 7, no. 18, pp. 2621–2628, 2011.

[40] J. H. M. Maurer, L. González-García, B. Reiser, I. Kanelidis, and T. Kraus, "Sintering of ultrathin gold nanowires for transparent electronics," *ACS Appl. Mater. Interfaces*, vol. 7, no. 15, pp. 7838–7842, 2015.

[41] J. Lee, I. Lee, T. S. Kim, and J. Y. Lee, "Efficient welding of silver nanowire networks without post-processing," *Small*, vol. 9, no. 17, pp. 2887–2894, 2013.

[42] T. B. Jones, *Electromechanics of Particles*. 2005.

[43] W. Ahmed, E. S. Kooij, A. Van Silfhout, and B. Poelsema, "Quantitative analysis of gold nanorod alignment after electric field-assisted deposition," *Nano Lett.*, vol. 9, no. 11, pp. 3786–3794, 2009.

[44] W. B. Russel, D. A. Saville, and W. R. Schowalter, *Colloidal Dispersions*.

Cambridge University Press, 1991.

[45] A. Ramos, *Electrokinetics and electrohydrodynamics in microsystems*, vol. 530. Springer Science & Business Media, 2011.

[46] M. Sam, "Field-directed assembly of nanowires: identifying directors, disruptors and indices to maximize the device yield," *Nanoscale*, vol. 8, no. 2, pp. 889–900, 2016.

[47] N. G. Green, A. Ramos, A. Gonz á lez, H. Morgan, and A. Castellanos, "Fluid flow induced by nonuniform ac electric fields in electrolytes on microelectrodes. I. Experimental measurements," *Phys. Rev. E*, vol. 61, no. 4, p. 4011, 2000.

[48] Y. Liu, J.-H. Chung, W. K. Liu, and R. S. Ruoff, "Dielectrophoretic assembly of nanowires," *J. Phys. Chem. B*, vol. 110, no. 29, pp. 14098–14106, 2006.

[49] K. H. Bhatt and O. D. Velev, "Control and modeling of the dielectrophoretic assembly of on-chip nanoparticle wires," *Langmuir*, vol. 20, no. 2, pp. 467–476, 2004.

[50] K. E. Korte, S. E. Skrabalak, and Y. Xia, "Rapid synthesis of silver nanowires through a CuCl-or CuCl 2-mediated polyol process," *J. Mater. Chem.*, vol. 18, no. 4, pp. 437–441, 2008.

[51] J. H. Lee, P. Lee, D. Lee, S. S. Lee, and S. H. Ko, "Large-scale synthesis and characterization of very long silver nanowires via successive multistep growth," *Cryst. Growth Des.*, vol. 12, no. 11, pp. 5598–5605, 2012.

[52] H. Mao, J. Feng, X. Ma, C. Wu, and X. Zhao, "One-dimensional silver nanowires synthesized by self-seeding polyol process," *J. Nanoparticle Res.*, vol. 14, no. 6, p. 887, 2012.

[53] Y. Sun, B. Mayers, T. Herricks, and Y. Xia, “Polyol synthesis of uniform silver nanowires: A plausible growth mechanism and the supporting evidence,” *Nano Lett.*, vol. 3, no. 7, pp. 955–960, 2003.

[54] R. Ramya, R. Sivasubramanian, and M. V Sangaranarayanan, “Conducting polymers-based electrochemical supercapacitors—progress and prospects,” *Electrochim. Acta*, vol. 101, pp. 109–129, 2013.

[55] G. Haacke, “New figure of merit for transparent conductors,” *J. Appl. Phys.*, vol. 47, no. 9, pp. 4086–4089, 1976.

[56] “Varian Cary ® 50 UV-Vis Spectrophotometer,” *2008*. [Online]. Available: www.agilent.com/chem. [Accessed: 06-Jul-2018].

[57] I. Miccoli, F. Edler, H. Pfnür, and C. Tegenkamp, “The 100th anniversary of the four-point probe technique: the role of probe geometries in isotropic and anisotropic systems,” *J. Phys. Condens. Matter*, vol. 27, no. 22, p. 223201, 2015.

[58] J. V van de Groep, P. Spinelli, and A. Polman, “Transparent Conducting Silver Nanowire Networks,” *Nano Lett.*, vol. 12, no. 6, pp. 3138–3144, 2012.

[59] M. Dressel and G. Grüner, “Electrodynamics of solids: optical properties of electrons in matter.” AAPT, 2002.

[60] S. De and J. N. Coleman, “The effects of percolation in nanostructured transparent conductors,” *Mrs Bull.*, vol. 36, no. 10, pp. 774–781, 2011.

[61] “Indium-Tin-Oxide Coated Substrates Technical Data Sheet.” [Online]. Available: https://www.2spi.com/ito-tech-data/. [Accessed: 06-Oct-2018].

[62] J. Lee, P. Lee, H. Lee, D. Lee, S. S. Lee, and S. H. Ko, “Very long Ag nanowire synthesis and its application in a highly transparent, conductive and flexible metal

electrode touch panel," *Nanoscale*, vol. 4, no. 20, pp. 6408–6414, 2012.

[63] S.-Y. Bae *et al.*, "Large-area graphene films by simple solution casting of edge-selectively functionalized graphite," *ACS Nano*, vol. 5, no. 6, pp. 4974–4980, 2011.

[64] H. Wu *et al.*, "Electrospun metal nanofiber webs as high-performance transparent electrode," *Nano Lett.*, vol. 10, no. 10, pp. 4242–4248, 2010.

[65] U.S. Geological Survey (USGS), "Silver Statistics and Information," 2018. [Online]. Available: https://minerals.usgs.gov/minerals/pubs/commodity/silver/. [Accessed: 30-Sep-2018].

[66] "Indium tin oxide coated glass slide." [Online]. Available: https://www.sigmaaldrich.com/catalog/product/aldrich/703184?lang=en&region=CA. [Accessed: 30-Sep-2018].

[67] G. E. Pike and C. H. Seager, "Percolation and conductivity: A computer study. I," *Phys. Rev. B*, vol. 10, no. 4, p. 1421, 1974.

[68] S. M. Bergin, Y.-H. Chen, A. R. Rathmell, P. Charbonneau, Z.-Y. Li, and B. J. Wiley, "The effect of nanowire length and diameter on the properties of transparent, conducting nanowire films," *Nanoscale*, vol. 4, no. 6, pp. 1996–2004, 2012.

[69] D. Stauffer and A. Aharony, *Introduction to percolation theory: revised second edition*. CRC Press, 2014.

[70] A. R. Madaria, A. Kumar, F. N. Ishikawa, and C. Zhou, "Uniform, highly conductive, and patterned transparent films of a percolating silver nanowire network on rigid and flexible substrates using a dry transfer technique," *Nano Res.*, vol. 3, no. 8, pp. 564–573, 2010.

[71] L. Hu, D. S. Hecht, and G. Grüner, "Percolation in transparent and conducting

carbon nanotube networks," *Nano Lett.*, vol. 4, no. 12, pp. 2513–2517, 2004.

[72] D. P. Langley *et al.*, "Metallic nanowire networks: effects of thermal annealing on electrical resistance," *Nanoscale*, vol. 6, no. 22, pp. 13535–13543, 2014.

[73] T. Tokuno *et al.*, "Fabrication of silver nanowire transparent electrodes at room temperature," *Nano Res.*, vol. 4, no. 12, pp. 1215–1222, 2011.

[74] J. a Spechler, K. a Nagamatsu, J. C. Sturm, and C. B. Arnold, "Improved efficiency of hybrid organic photovoltaics by pulsed laser sintering of silver nanowire network transparent electrode.," *ACS Appl. Mater. Interfaces*, vol. 7, no. 19, pp. 10556–62, 2015.

[75] E. C. Garnett *et al.*, "Self-limited plasmonic welding of silver nanowire junctions.," *Nat. Mater.*, vol. 11, no. 3, pp. 241–9, 2012.

[76] T. Song *et al.*, "Nanoscale joule heating and electromigration enhanced ripening of silver nanowire contacts," *ACS Nano*, vol. 8, no. 3, pp. 2804–2811, 2014.

[77] W. Jeong, K. Kim, Y. Kim, W. Lee, and P. Reddy, "Characterization of nanoscale temperature fields during electromigration of nanowires.," *Sci. Rep.*, vol. 4, p. 4975, 2014.

[78] A. Kumar, N. S. Vidhyadhiraja, and G. U. Kulkarni, "Current distribution in conducting nanowire networks," *J. Appl. Phys.*, vol. 122, no. 4, p. 45101, 2017.

[79] S. Ye, A. R. Rathmell, Z. Chen, I. E. Stewart, and B. J. Wiley, "Metal nanowire networks: The next generation of transparent conductors," *Adv. Mater.*, vol. 26, no. 39, pp. 6670–6687, 2014.

[80] A. Vafaei, A. Hu, and I. A. Goldthorpe, "Joining of individual silver nanowires via electrical current," *Nano-Micro Lett.*, vol. 6, no. 4, pp. 293–300, 2014.

[81] A. Vafaei, A. Hu, and I. A. Goldthorpe, “Joining of individual silver nanowires via electrical current,” *Nano-Micro Lett.*, vol. 6, no. 4, pp. 293–300, 2014.

[82] P. W. Fan, W. L. Chen, T. H. Lee, Y. J. Chiu, and J. T. Chen, “Rayleigh-instability-driven morphology transformation by thermally annealing electrospun polymer fibers on substrates,” *Macromolecules*, vol. 45, no. 14, pp. 5816–5822, 2012.

[83] S. Karim *et al.*, “Influence of crystallinity on the Rayleigh instability of gold nanowires,” *J. Phys. D. Appl. Phys.*, vol. 40, no. 12, pp. 3767–3770, 2007.

[84] N. Moghimian, “Electrochemical Control for Nanoelectromechanical Device Production,” University of Victoria, 2015.

[85] M. Sam, J. Alsaif, and R. B. Bhiladvala, “Fabrication of Flexible Transparent Electrodes by Using Field-Assisted Nanowire Chaining,” in *SID Symposium Digest of Technical Papers*, 2017, vol. 48, no. 1, pp. 1463–1465.

Appendix A Technical discussions of Haacke's FOM

FOM is usually defined as the ratio of some form of *T* to some form of R_s, thus the simplest form of FOM (F) is:

$$F = \frac{T}{R_s}, \tag{24}$$

R_s of a transparent conductive film can be expressed as:

$$R_s = \frac{1}{\sigma t}, \tag{25}$$

where σ is the electrical conductivity, and *t* is the film thickness. The transmittance of the film is also related to the thickness:

$$T = e^{-\alpha t}, \tag{26}$$

where α is the optical absorption coefficient. Combining the three equations above yields:

$$F = \sigma t e^{-\alpha t}, \tag{27}$$

To find the optimal thickness, $t_{optimal}$, that allows the maximum *F*, solve the following equation:

$$\frac{\partial F}{\partial t} = 0 \tag{28}$$

which results in $t_{optimal} = \frac{1}{\alpha}$, and the corresponding second derivative of *F* with respect to *t* is negative, which means F is maximized. The corresponding transparency *T* = 37%. This transparency is too low for applications practiced. Therefore, FOM needs to be redefined. Redefine FOM as:

$$F = \frac{T^x}{R_s}, \tag{29}$$

in which the factor $x > 1$ in order to better balance transparency and sheet resistance. Solving equation (28) again, the optimal thickness is now $t_{optimal} = \frac{1}{x\alpha}$, and the corresponding transparency is $T = e^{-\frac{1}{x}}$. Matching this transparency with the benchmark TE transparency, 90%, yields x = 9.49. Since 10 is a close integer that is favorable in calculation, the factor 10 is chosen to define the Haacke's FOM.

Appendix B Procedures of photolithography and lift-off process

Preparation	Create mask with L-Edit and produce the mask
	Clean a 4 inch × 4 inch glass substrate with acetone, IPA and DI water, dry it with nitrogen gas
	Dehydrate (bake) the glass substrate at 110°C for 1 min, and then cool down for 4min in room temperature
Photolithography	Spin coat LOR-2A photoresist on the substrate at 3000 RPM for 45 sec
	Bake the substrate at 180 °C for 2 min, and then cool down for 4min at room temperature
	Spin coat AZ703 photoresist on the substrate at 4000 RPM for 1min
	Pre-bake the substrate at 90 °C for 1 min, and then cool down for 4min at room temperature
	Pre-bake the substrate again at 110 °C for 1 min, and then cool down for 4min at room temperature
	Exposed the substrate with photoresist under the mask to UV light for 1.5 sec
	Post-bake the substrate at 110 °C for 1 min, and then cool down for 4min at room temperature
	Develop the photoresist in developer MIF 300 for 32 sec, and then rinse it with DI water and dry it with nitrogen gas
Deposit	Deposit 10nm of titanium followed by 50nm of gold using an evaporator or a sputtering machine

Lift-off	Soak the substrate in Microposit remover 1165 for 24 hours at room temperature
	Rinse the substrate with DI water, and then dry it with nitrogen gas

Appendix C Current and heating power distribution over chained networks and branched networks

These tables show calculation results from Matlab Simulink; The applied current is 3I.

Table C.1 Current and power distribution in chained networks when R6=2R.

NW chains			
Resistor NO.	Resistance	Current (I)	Power (RI^2)
1	R	1.0713	1.1477
2	R	1.0713	1.1477
3	R	1.0713	1.1477
4	R	1.0713	1.1477
5	R	0.8571	0.7346
6	2R	0.8571	1.4692
7	R	0.8571	0.7346
8	R	0.8571	0.7346
9	R	1.0713	1.1477
10	R	1.0713	1.1477
11	R	1.0713	1.1477
12	R	1.0713	1.1477

Current and power distribution in branched network when R6=2R and all the other resistors have the same resistance, R.

Table C.2 Current and power distribution in branched network when R6=2R.

NW networks			
Resistor NO.	Resistance	Current (I)	Power (RI^2)
1	R	1.0383	1.0781
2	R	1.1529	1.3292
3	R	1.0323	1.0656
4	R	1.008	1.0161
5	R	0.9234	0.8527
6	2R	0.6942	0.9638
7	R	0.9357	0.8755
8	R	0.984	0.9683
9	R	1.0383	1.0781
10	R	1.1529	1.3292
11	R	1.0323	1.0656
12	R	1.008	1.0161
13	R	-0.1152	0.0133
14	R	0.1206	0.0145
15	R	0.024	0.0006
16	R	0.1152	0.0133
17	R	-0.1206	0.0145
18	R	-0.024	0.0006

Table C.3 Current and power distribution in chained networks when R6=0.5R.

NW chains			
Resistor NO.	Resistance	Current (I)	Power (RI^2)
1	R	0.9546	0.9113
2	R	0.9546	0.9113
3	R	0.9546	0.9113
4	R	0.9546	0.9113
5	R	1.0908	1.1898
6	0.5R	1.0908	0.5949
7	R	1.0908	1.1898
8	R	1.0908	1.1898
9	R	0.9546	0.9113
10	R	0.9546	0.9113
11	R	0.9546	0.9113
12	R	0.9546	0.9113

Table C.4 Current and power distribution in branched networks when R6=0.5R.

NW networks			
Resistor NO.	Resistance	Current (I)	Power (RI^2)
1	R	0.9648	0.9308
2	R	0.8586	0.7372
3	R	0.9702	0.9413
4	R	0.9927	0.9855
5	R	1.0707	1.1464
6	0.5R	1.2825	3.2896
7	R	1.0596	1.1228
8	R	1.0149	1.0300
9	R	0.9648	0.9308
10	R	0.8586	0.7372
11	R	0.9702	0.9413
12	R	0.9927	0.9855
13	R	0.1059	0.0112
14	R	-0.1116	0.0125
15	R	-0.0222	0.0005
16	R	-0.1059	0.0112
17	R	0.1116	0.0125
18	R	0.0222	0.0005

Appendix D COMSOL simulation results over different gap sizes

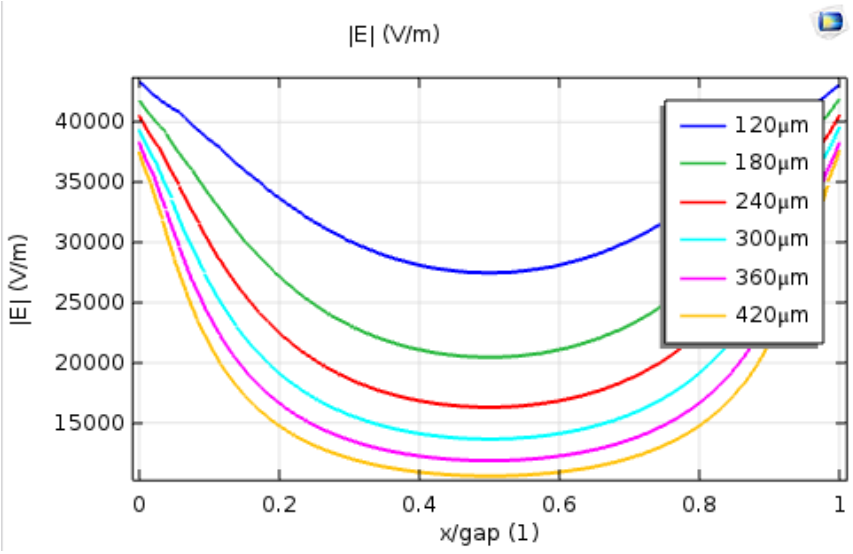

Figure D.1 The distribution of the electric field strength over the gap between electrodes on PET with a thickness of 23µm. The applied frequency is 1MHz.

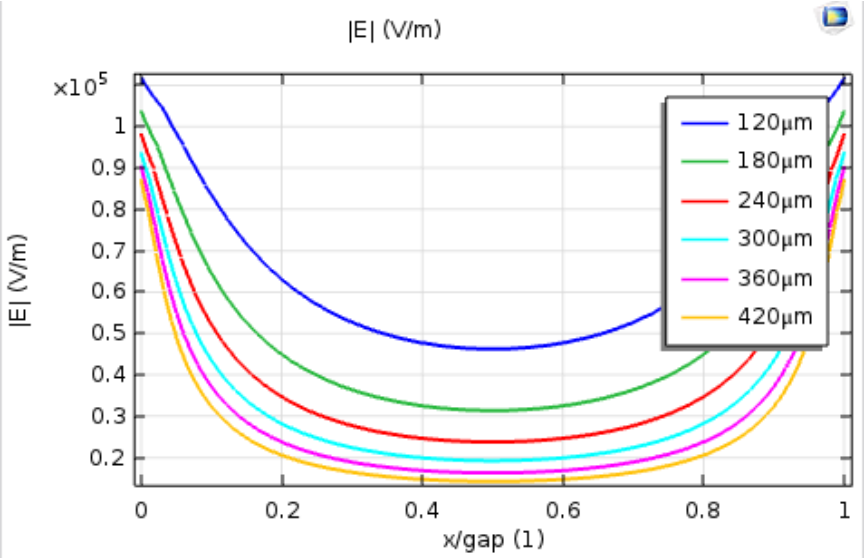

Figure D.2 The distribution of the electric field strength over the gap between electrodes on polyimide with a thickness of 7µm. The applied frequency is 100kHz.

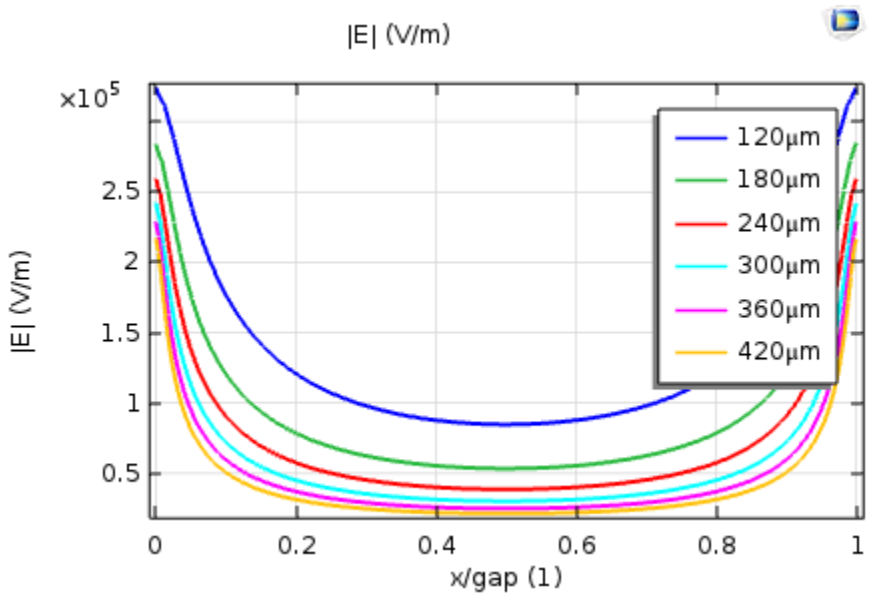

Figure D.3 The distribution of the electric field strength over the gap between electrodes direct on the glass substrate with electrodes. The applied frequency is 10kHz.

Appendix E COMSOL results on PET with different thickness

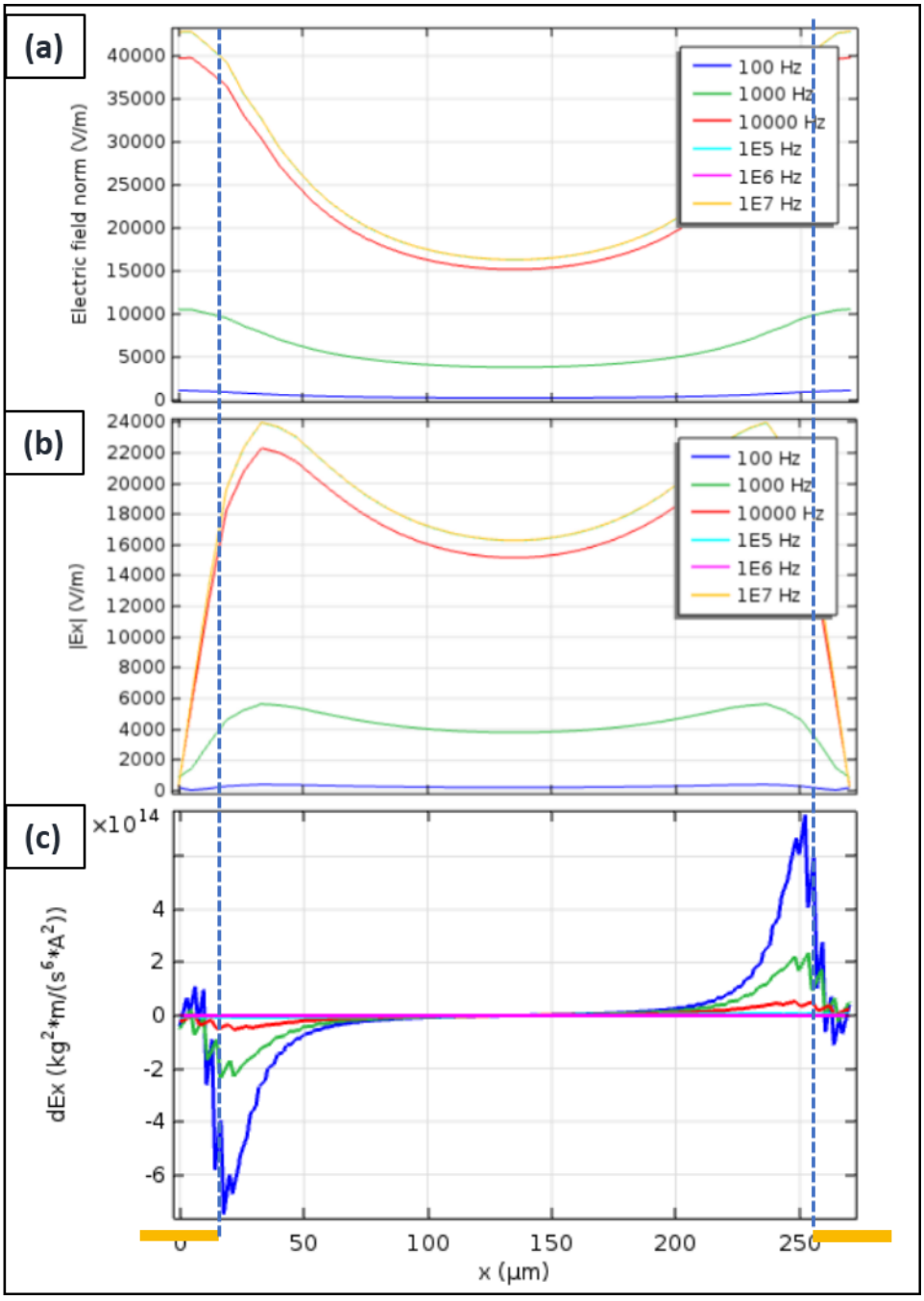

Figure E.1 The (a) electric field strength ($|E|$), (b) x component of the electric field ($|E_x|$), and (c) x component of the electric field gradient ($dE_x=\partial|E|^2/\partial x$), on PET with different polymer thickness. The gap size is chosen as 240µm, and the applied frequency is 1MHz.

Appendix F Figures of NW networks

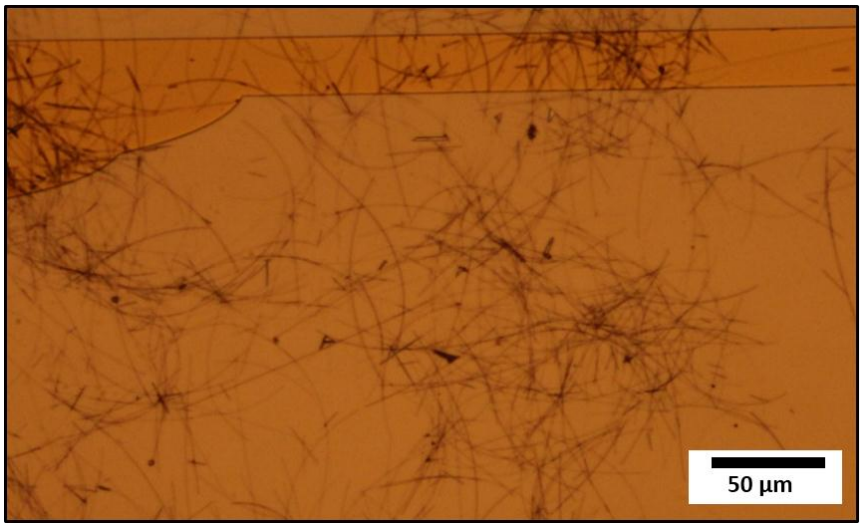

Figure F.1 Random NW networks created on polyimide in the experiment process described in Chapter 2, but no electric field is applied. The NW concentration was 0.25 mg/mL.

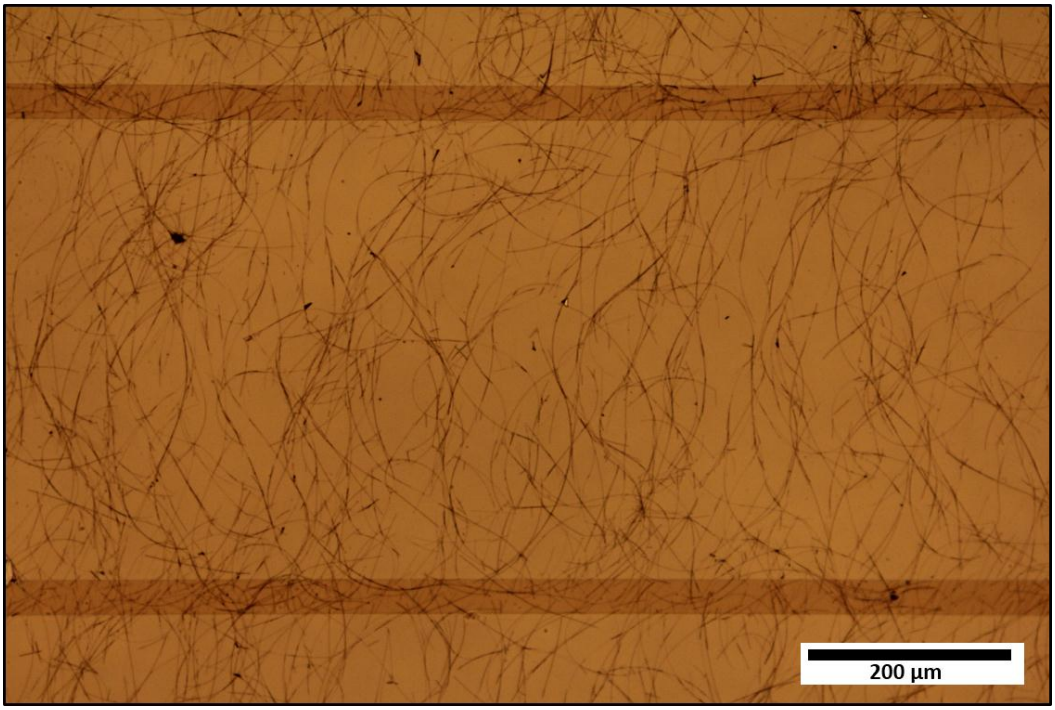

Figure F.2 Ordered Ag NW networks on polyimide fabricated with sandwiched channels. The gap size is 420µm.

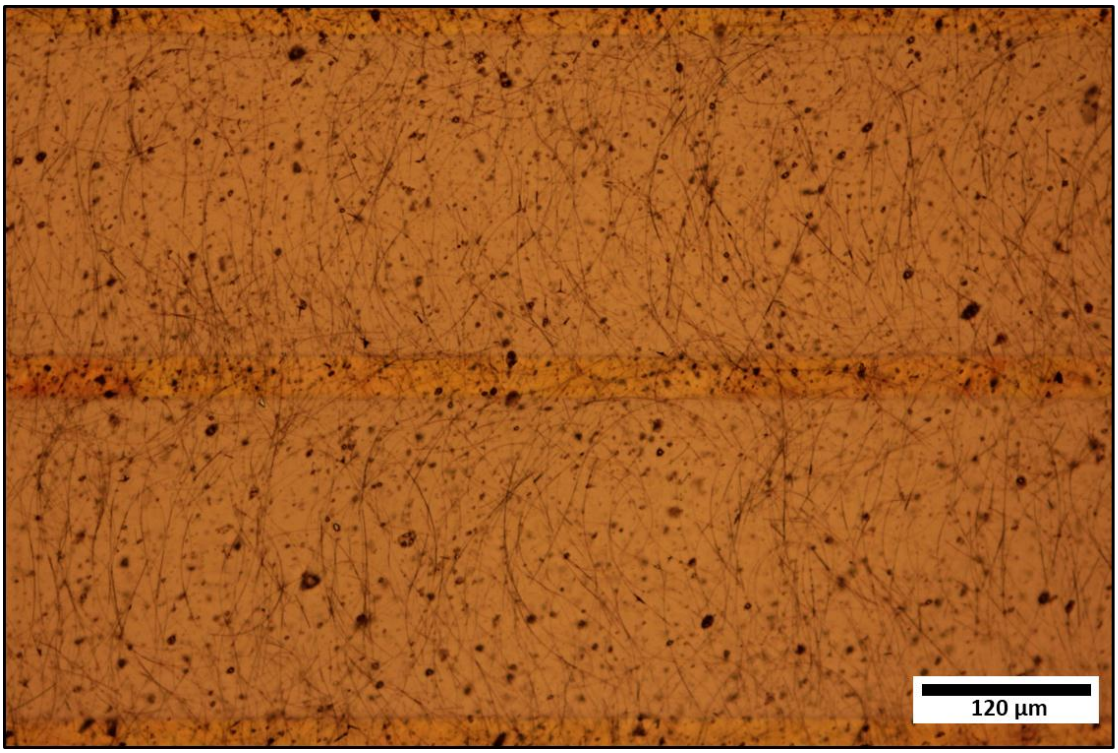

Figure F.3 Ordered Ag NW networks on PET fabricated with sandwiched channels. The gap size is 240µm.

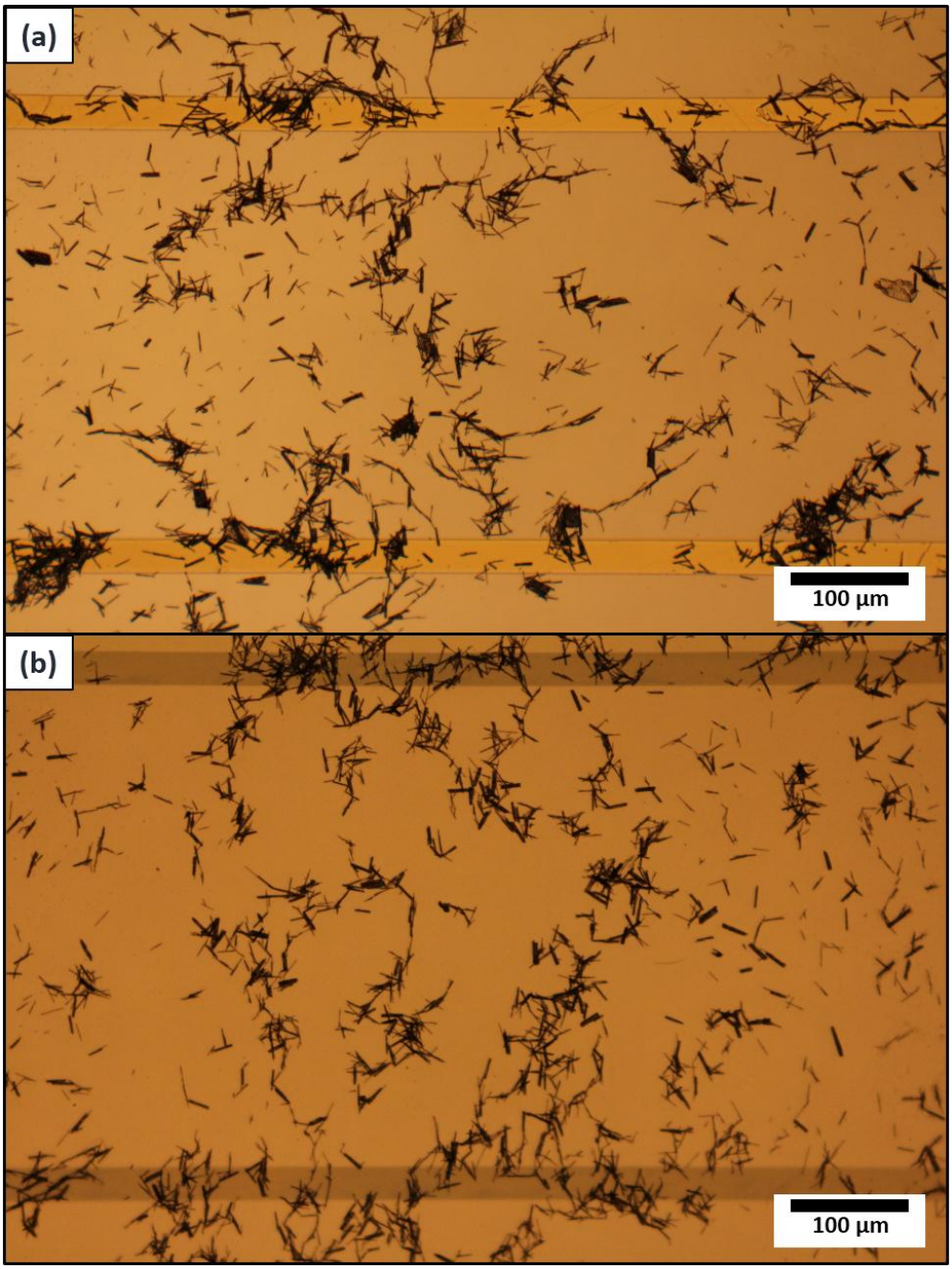

Figure F.4 NW chaining experiment results using open channels with gap sizes of (a) 360µm, (b) 420µm on polyimide substrate. The NWs used were Rh NWs with an average length of 6µm. The applied voltage and frequency were 7V and 100kHz, respectively.